AN ABSTRACT OF THE THESIS OF

Joyce D. Hawthorne for the Master of Science Degree in Physical Science presented on August 10, 1981.

Title: Neutron Diffraction of Samarium Deuteride

Abstract approved: Charles Grandy

Studies are being performed on the crystal structure of rare earth metal hydrides for use as hydrogen storage systems. As hydrogen is added to the metal, a face centered cubic hydride is formed. Additional hydrogen is then absorbed and the metal lattice reduces its size. In the lighter rare earths, this reduction in lattice size appears to a stoichiometry of $MH_{3.0}$. With samarium and the heavier rare earths, the face centered cubic absorbs hydrogen and then undergoes a solid phase transition to a hexagonal structure capable of absorbing hydrogen up to the $MH_{3.0}$ limit.

The location of the hydrogen atoms within the cubic and hexagonal phases around the transition is the focus of this project. These atom positions can best be detected by neutron diffraction techniques applied to different stoichiometries, both cubic and hexagonal, bracketing the transition. The experiments were performed on samarium-154 deuteride.

My part in this ongoing research involve first designing and building a system of known volume. Then, different stoichiometric samples of samarium deuteride, using determined P-T-C conditions, were

prepared. A neutron diffraction pattern was run on each sample. Interpretation of this pattern provided an analysis of the hydrogen locations in the cubic and hexagonal crystal lattices.

NEUTRON DIFFRACTION OF SAMARIUM DEUTERIDE

A Thesis

Presented to

the Division of Physical Sciences

EMPORIA STATE UNIVERSITY

In Partial Fulfillment

of the Requirements for the Degree

Master of Science

---

by

Joyce Donelle Hawthorne

August 1981

Charles M. Grinley
Approved for the Major Department

Harold E. Durst
Approved for the Graduate Council

This thesis was performed

under the auspices

of the

LOS ALAMOS NATIONAL LABORATORY

of the

UNIVERSITY OF CALIFORNIA

PREFACE

The characterization by neutron diffraction of the cubic and hexagonal samarium deuterides is outlined in this thesis. Some background of lanthanide hydrides as well as samarium hydrides is reported. Some basic crystallography and analysis of diffraction patterns is presented. The preparation of the samarium deuterides is described followed by the procedures used in obtaining and analyzing the diffraction patterns. Detailed results are provided in graphical and table form.

The research presented opens up additional questions which will be analyzed further.

Gratitude goes to the Los Alamos National Laboratory for its graduate assistant program that enabled me to perform this research.

Appreciation goes to Dale Tuggle without whom this work would never have been possible and whose knowledge and supervision was superb. Also appreciation is extended to Bob Von Dreele who provided the computer programs utilized in the analysis and gave expert advice. Appreciation goes to John Yarnell who built the diffractometer and whose help was invaluable.

There were many others who are to be thanked for their help and support. Among them are Helen Fuller for computer assistance, David Abelman for drawing some of the figures, Cyntha Robison for typing the thesis, and the staff of WX-5 who helped me build and maintain the hydride preparation system.

TABLE OF CONTENTS

LIST OF TABLES

LIST OF FIGURES

SECTION 1

INTRODUCTION

Hydrogen reacts with the rare earth metals to form dihydrides with properties very different from the metals. These dihydrides can absorb more hydrogen to a limit corresponding to the trihydride composition. Hydrogen's use as a viable energy source would require the use of safer, more compact storage systems than pressurized tanks or liquid storage.[1-3] Rare earth metals and alloys can store hydrogen and release it by dissociation on demand. For this reason, the structure of the rare earth hydride systems are being characterized in detail.

The light lanthanide dihydrides have cubic structures that become more dense as they absorb more hydrogen. The heavier lanthanide dihydrides also become denser as they absorb additional hydrogen, but at some point during the absorbtion, they transform from the face centered cubic structure to a hexagonal structure. The face centered form of several rare earth hydrides have been characterized by x-ray diffraction and in the case of cesium hydride by neutron diffraction. Some x-ray diffraction has been performed on holmium trihydride in its hexagonal form.

It is the purpose of this work to try to characterize by neutron diffraction both the face centered cubic and the hexagonal phase of the samarium hydrides. It is hoped that this will help lay further foundations for solid state hydrogen storage systems.

SECTION 2

LITERATURE SEARCH

2.1 Lanthanide Metal Hydrides

All rare earth metals react exothermally with hydrogen to form hydrides. These hydrides have very different properties from their parent metals. Most are black, brittle flakes that crumble easily and are pyrophoric.

With the exception of europium and ytterbium, all the lanthanides can form a dihydride of the formula MH_2. X-ray diffraction measurements of several lanthanide dihydrides[4-5] and a neutron diffraction of cerium dihydride[6] show the dihydride to have the fluorite structure shown in Figure 1 with the metal atoms at the positions (0,0,0) and the face centering positions (0, ½, ½). The hydrogen is located in the tetrahedral holes at the positions (¼, ¼, ¼).

If the hydrogen pressure is high enough, the dihydride dissolves more hydrogen and can reach a maximum composition of MH_3. The additional hydrogen goes into the octahedral holes at the centers of the edges of the cubes at the (0, 0, ½) positions to form the bismuth trifluoride structure shown in Figure 2.

The first three lanthanides: lanthanum, cerium, and praseodymium, absorb hydrogen to the trihydride limit keeping the face centered cubic structure. There is evidence that neodymium acts as the heavier rare earths.[7] Samarium and the heavier lanthanides, at some stoichiometry above the face centered dihydride, transform into a

Figure 1: The fluorite structure. Dark circles represent metal atoms. Light circles represent hydrogen atoms.

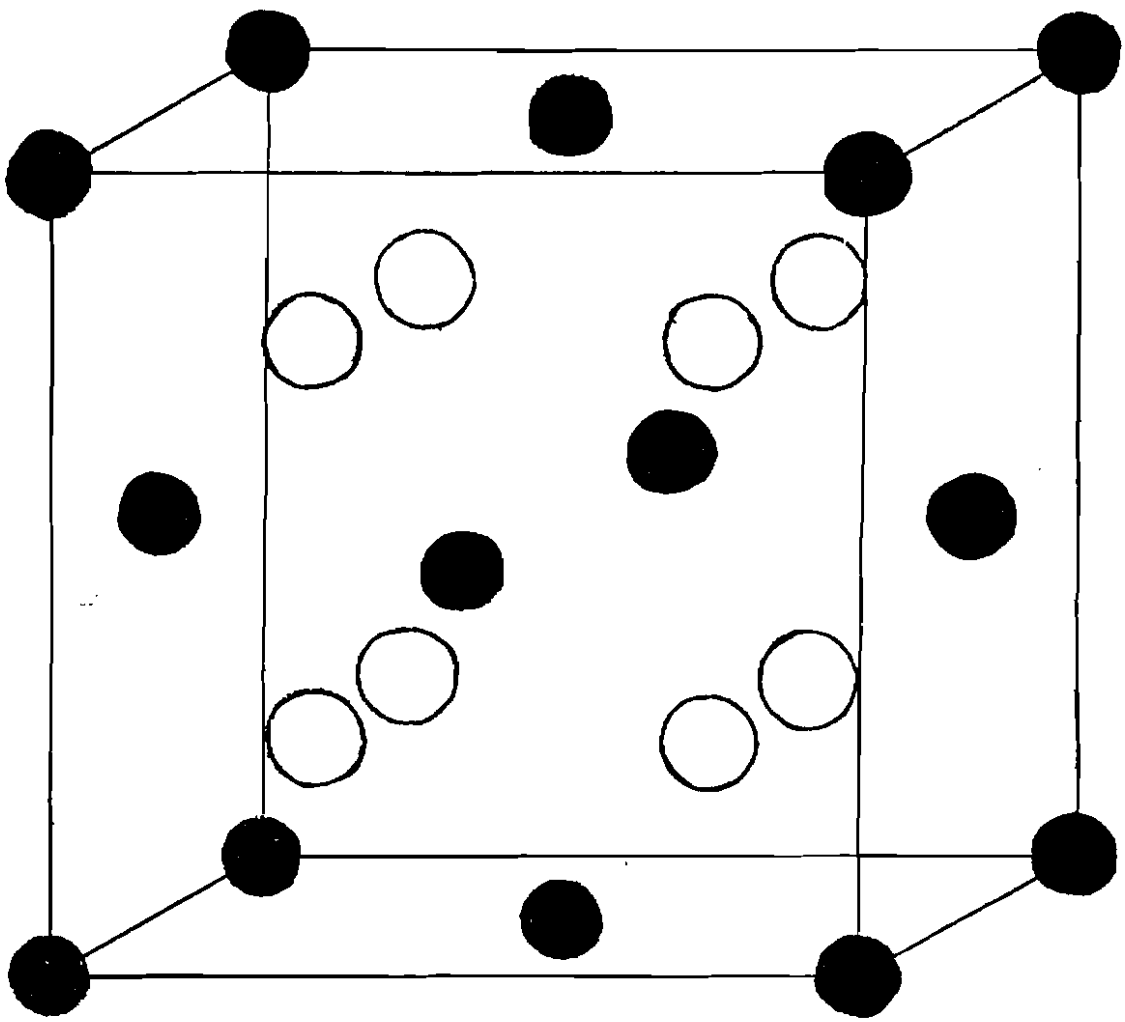

Figure 2: The bismuth trifluoride structure. Dark circles represent metal atoms. Light circles represent hydrogen atoms.

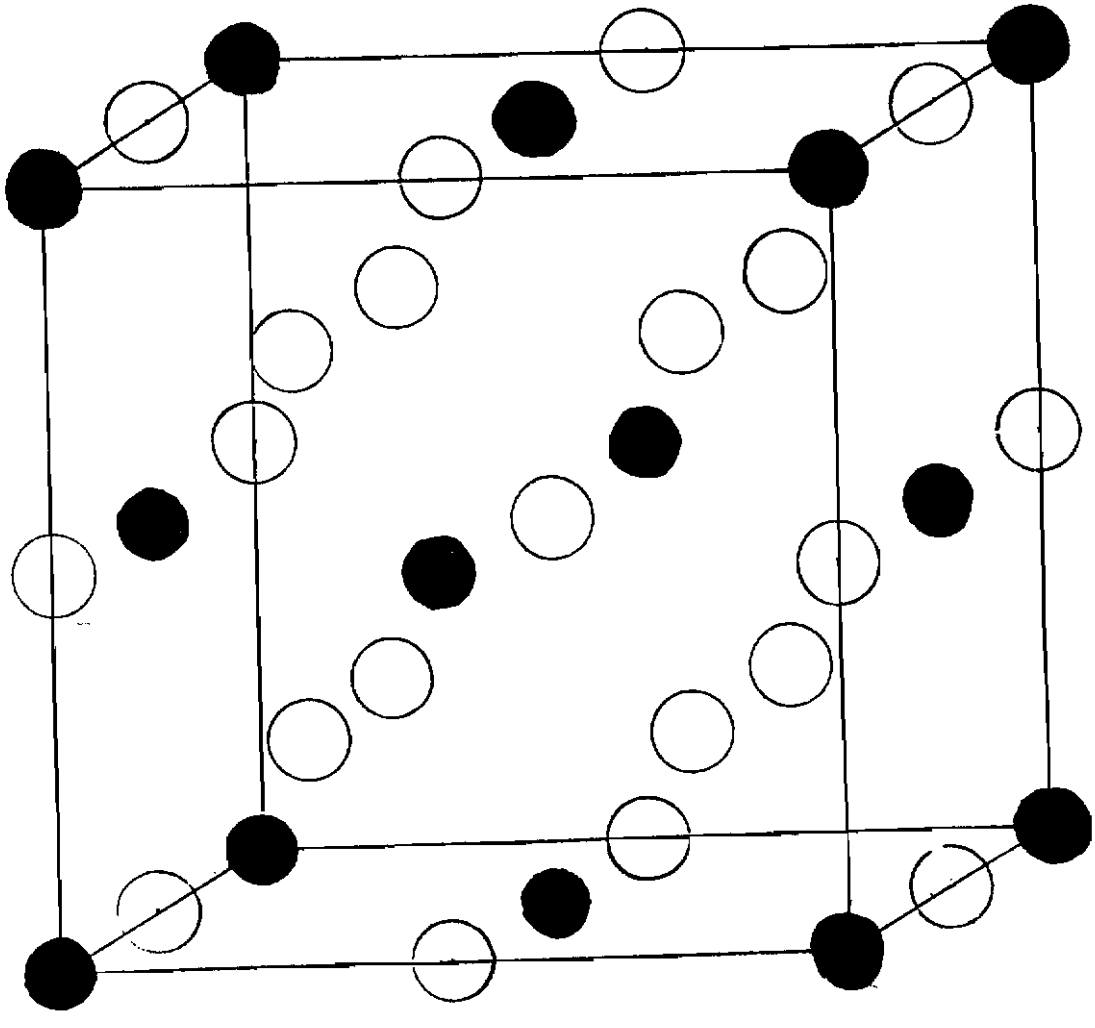

closepacked hexagonal structure. A neutron diffraction study of the hexagonal structure has been performed on holmium trihydride by Mansmann and Wallace.[8] They proposed a hexagonal structure of space group P_3cl (D_3^4d) using a unit cell of six molecules at these positions:

6 Ho in (j): (2/3 0 ¼; 0 2/3 ¼; 1/3 1/3 ¼)

12 D in (g): (x y z; y x-y z; y-x x z;
y x ½+z; x x-y ½+z;
y-x y ½+z) with x = 0.36,
y = 0.03, z = 0.095

4 D in (d): ± (1/3 2/3 z; 1/3 2/3 ½+z)
with z = 0.175

2 D in (a): ± (0 0 ¼).

The hydrogen radius is smaller than expected. Therefore, the tetrahedral hydrogens are slightly displaced from their ideal positions. "The actual HoH_3 structure is obtained by also displacing the octahedral hydrogens from their positions between the holmium planes into these planes. Only one third actually reach these planes, the other two thirds stay slightly out of these planes" to avoid close contact with the tetrahedral hydrogens. Mansmann and Wallace suggest that the other rare earth trihydrides might have this structure.

As the rare earth metals absorb more hydrogen beyond the dihydride limit, the lattice size decreases and the density increases. This phenomena is known as the lanthanide contraction.[9] It has not been determined whether this contraction is also present in the hexagonal phase.

2.2 Samarium Hydrides

X-ray diffraction measurements show that samarium hydride forms a face centered cubic dihydride with the fluorite structure. The dihydride structure has four samarium atoms at (0, 0, 0) and (0, ½, ½) and eight hydrogens in the tetrahedral positions at (¼, ¼, ¼).

The lattice size for $SmH_{2.0}$ as measured by x-ray diffraction is a = 5.376 ± 0.003 A.[10] Using this value, the x-ray density is calculated to be 6.52 g per cc.[11] The metal-hydrogen distance calculated from x-ray diffraction data is 2.328 A,[12] but there is disagreement about the sizes of the samarium and hydrogen ions. A summary of ionic radii and metal-hydrogen distances of the dihydride given by various authors is given in Table 1.

X-ray diffraction shows that samarium dihydride, like the other rare earth dihydrides can take on additional hydrogen. The hydrogen goes into the octahedral holes of the fluorite structure. The Sm^{+3} radius in the trihydride determined by Holley, Mulford, Ellinger, Koehler, and Zachariesen[13] is 1.804 A.

As the stoichiometry increases above 2.0, the lattice size decreases and interplanar distances decrease. Pebler and Wallace[14] note that the lattice size of $SmH_{1.9}$ is a = 5.376 A but decreases to a = 5.34 A at $SmH_{2.7}$. They explain the contraction by proposing that the conduction electrons of the metal ions repel each other, increasing the metal lattice size and weakening the electrostatic interaction of oppositely charged components. Then when hydrogen is introduced, the electrons are tied up and interaction between the samarium and hydrogen ions increase and pulls the molecule together forming a denser structure.

TABLE 1

IONIC RADII AND M-H DISTANCES FOR SMH

Samarium Radius	Tetrahedral Hydrogen Radius	M-H Distance	References
1.751	0.577	2.328	a
0.97	1.28	2.25	b
1.90	0.43	2.33	c
1.95	0.38	2.33	d
0.96	1.40	2.36	e

Values in Angstroms

a Holley, Mulford, Ellinger, Koehler, and Zachariesen, J. Phys. Chem. 59, 1226 (1955)

b Libowitz and Gibb, J. Phys. Chem. 60, 510 (1956)

c Denver Research Institute, "Investigation of Hydriding Characteristics of Intermetallic Compounds", Summary Report LAR-55 USAEC (1961) (Paulings Method)

d Denver Research Institute, Ibid (Bond Distances)

e Gibb and Schumacher, J. Phys. Chem. 64, 1407 (1960)

Pebler and Wallace[15] found the cubic to hexagonal transition to occur at $SmH_{2.59}$. The lattice sizes for the hexagonal are a = 3.72 A and c = 6.779 A.

Pebler and Wallace[16] propose an explanation for the transformation in terms of the lattice contraction. Pairs of tetrahedral hydrogen ions move closer during the contraction to a separation of 1.5 A. Since the radius of the hydrogen ion is 0.65 A, the ions are only 0.2 A apart and a strong repulsion occurs. To relieve the stress, the crystal transforms to the hexagonal phase. This transformation also results in an additional density reduction of ten percent.

Pebler and Wallace[17] locate the boundaries of the two phase region at $SmH_{2.53}$ and $SmH_{2.59}$. Messer and Park[18] determine the transition boundaries to be $SmH_{2.5}$ and $SmH_{2.7}$ while Mintz, Hierschler and Hadari[19] record $SmH_{2.4}$ and $SmH_{2.85}$.

Messer and Park[20] in 1972 performed extensive work on the decomposition pressure versus temperature of the samarium-hydrogen system. The measured transition pressure was lower as the temperature ascended and higher as the temperature descended. This hysteresis loop shown in Figure 3 is found in other hydrides and shows the lower equilibrium pressure of the hexagonal phase, which is more stable at the lower temperature. They estimate the "true, reversible" transition temperature to occur just below the rapid rise in pressure on the warming runs as shown in Figure 3 and the transition pressure to occur just below the lowest pressure on the hexagonal side of the plateau as shown in Figure 4. The transition at 250°C and 300°C occur at 70mm and 475mm, respectively, as read from the graph in Figure 4.

Figure 3: Pressure versus temperature of the samarium-hydrogen system. ⟶ ascending temperature; ⟵ descending temperature. Taken from Messer and Park, J. Less-Common Metals 26, 235, 1972.

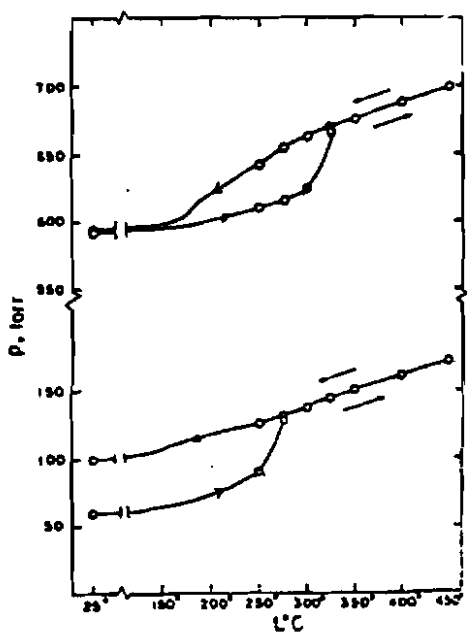
700
650
600
550
p, torr
150
100
50
25°
150°
200°
250°
300°
350°
400°
450°
t°C

Figure 4: Dissociation pressure versus H/Sm. Taken from Messer and Park, J. Less-Common Metals 26, 235, 1972.

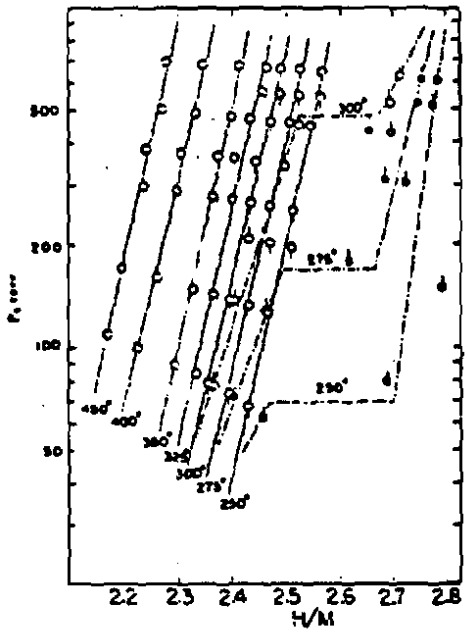
300
200
100
50
2.2
2.3
2.4
2.5
2.6
2.7
2.8
H/M
300°
275°
250°
450°
400°
350°
325°
300°
275°
250°

Mintz, Hadari and Bixon[21] do not estimate the two phase transition plateau but report the heating plateau at 350°C and the cooling plateau at 270°C for both pressures equal to approximately 700mm. These values were later corrected by Mintz, Hierschler, and Hadari[22] to 314 ± 5°C on heating and 230 ± 5°C on cooling.

Dissociation information was provided by Korst and Warf[23] for the dihydride between compositions of $SmH_{1.95}$ and $SmH_{2.1}$ as shown in Figure 5. Messer and Park[24] performed dissociation experiments for stoichiometries between $SmH_{2.2}$ and $SmH_{2.8}$. Their results are shown in Figure 4. Mintz[25] produced one curve of the temperature-composition graph between stoichiometries of $SmH_{2.0}$ and $SmH_{2.8}$. Their work is shown in Figure 6.

Greis, Knappe and Muller[26] performed x-ray diffraction analysis on the samarium hydrides and deuterides. Besides the cubic and hexagonal phases, a new tetragonal phase was reported to exist between the cubic and hexagonal forms. This new phase had a tetragonal structure of space group I 4/m with 2 atoms per unit cell. The intermediate phase occurs at lower room temperature equilibriums while the phase relationships previously reported occur at high temperatures.

Greis, Knappe and Muller[27] determine the cubic to exist for compositions at $SmH_{1.95-2.34}$ for high temperature equilibrium and at $SmH_{1.95-2.28}$ for low temperature equilibrium. They determine the lattice parameters for the Sm_3H_7 to be a = 3.7780 A and c = 5.3647 A and for Sm_3D_7 to be a = 3.7716 A and c = 5.3503 A. The hexagonal parameters for SmH and SmD are respectively, a = 3.7870 A and c = 6.7926 A and a = 3.7726 A and c = 6.7632A.

Figure 5: Dissociation Pressure Isotherms for some rare earth-deuterium systems. Taken from Korst and Warf, Inorg. Chem. 5, 1719, 1966.

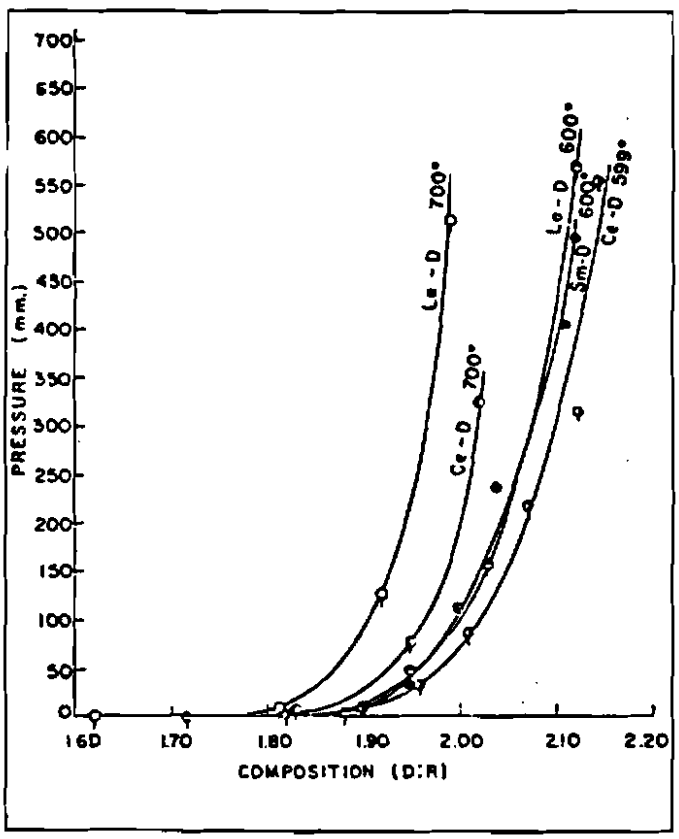
PRESSURE (mm.)
700
650
600
550
500
450
400
350
300
250
200
150
100
50
0
1.60
1.70
1.80
1.90
2.00
2.10
2.20
COMPOSITION (D:R)
La - D 700°
Ce - D 700°
La - D 600°
Sm-D 600°
Ce - D 599°

Figure 6: Temperature-composition graph by thermal analysis of the samarium-hydride system. —·—·— First cooling; ——— Heating from room temperature to 600°C; ----Cooling from 600°C to room temperature. Taken from Mintz, "Thermodynamics and Statistical Mechanics of Some Hydrides of the Lanthanides and Actinides". NRCN-398 Israel Atomic Energy Commission; 1976, pp108.

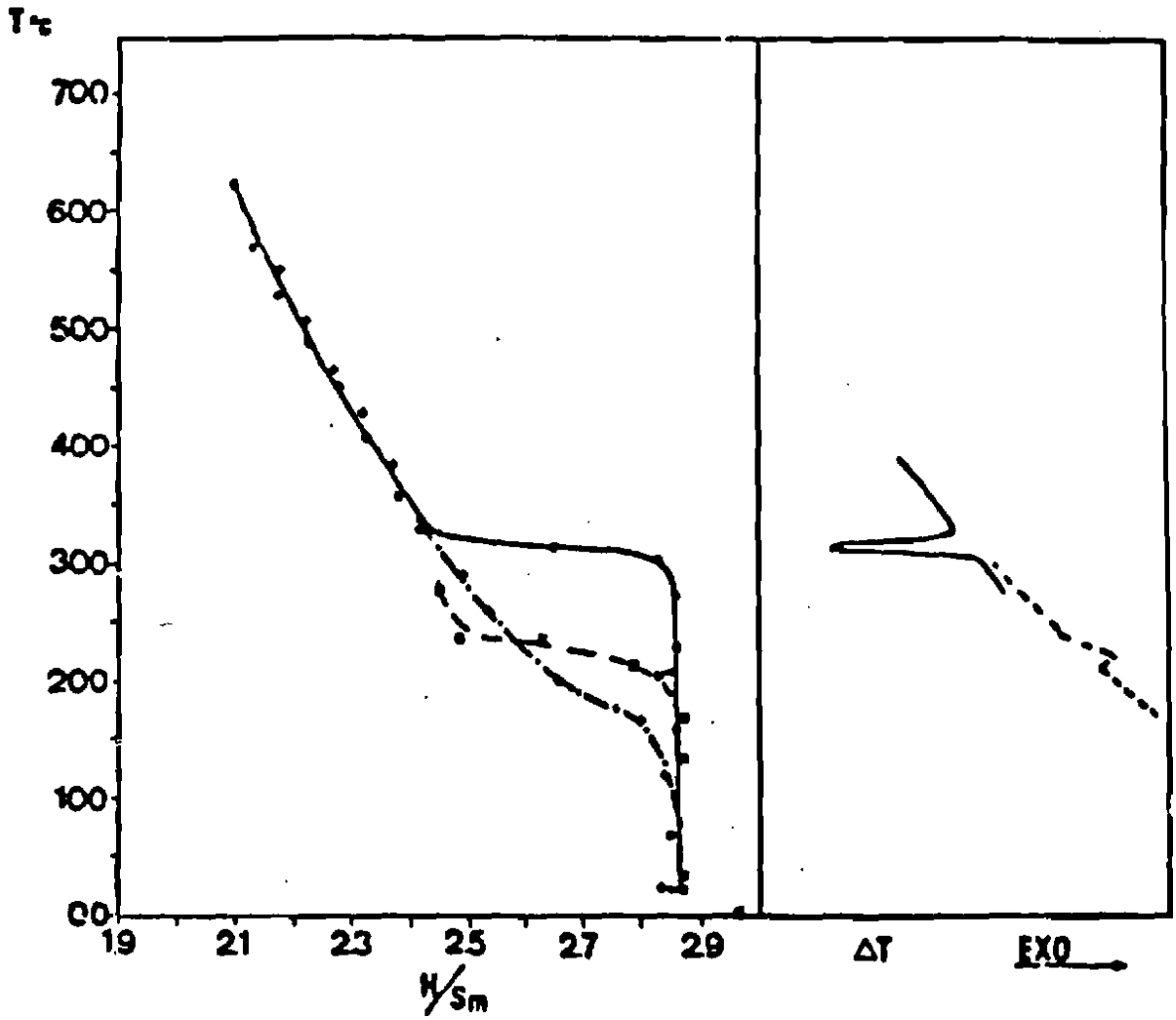
T °C
700
600
500
400
300
200
100
00
19
21
23
25
27
29
H/Sm
ΔT
EXO

No superstructure reflections were seen in the hexagonal or tetragonal samples.

The phase diagrams and pressure-temperature-composition information for the samarium hydrides have not been fully developed.

2.3 Magnetic Characteristics of Samarium Hydrides

The magnetic characteristics are considered by Kubota and Wallace[28] who found no magnetic ordering for either the cubic and hexagonal samarium hydrides between 4.2 K and 300 K.

2.4 Hydride Preparation Techniques

In general all preparative techniques for samarium hydrides involve direct contact of the metal with the hydrogen in a closed system. Some means of measuring the temperature and the pressure in the system is provided. The stoichiometries are determined using the ideal gas law and the measured amounts of the samarium metal.

Samarium metal is easily oxidized and especially sensitive to air and moisture. The reaction of the metal with the hydrogen is greatly inhibited by any surface film, so the metal surface is cleaned and prepared under some inert gas or mineral oil and loaded into glass containers. The metal is weighed accurately in either the inert gas, the oil, or in a vacuum. The metal is then degassed in a vacuum system for several hours with or without heat and then heated to the reaction temperatures desired. Hydrogen is then admitted to the system for reaction. In most cases the reaction starts immediately but the reaction time is related directly to the surface film. The reaction will occur at any temperature if sufficient time is allowed for it to diffuse through any film present.

The hydrides can be produced by direct reaction to the desired stoichiometry or taken to a stoichiometry higher than desired and after the reaction is completed, dissociated to the desired stoichiometry. Whatever the temperatures and pressures of the reaction, all samples were left to anneal for hours to days to ensure equilibrium conditions.

Specific descriptive procedures of several researchers can be found in their respective works.[29-35]

SECTION 3

THEORY

3.1 Crystallography

Constructive and destructive interference takes place when waves are reflected from a series of planes. Bragg noted that constructive interference had its maximum intensity when, for a particular direction, the parallel rays left the planes at the same angle they originally entered and when the path difference of the waves reflected from successive planes was equal to the wavelength or a multiple of the wavelength of the wave. The path difference for waves reflected off different planes, shown in Figure 7, is AB + BC or 2AB. This distance can also be expressed as $AB = d(\sin\theta)$ where d is the distance between the two planes. The full expression for the Bragg equation becomes

$$n\lambda = 2\ d\ \sin\theta \qquad (1)$$

The same interference phenomena can be shown to be true for arrays of points in a lattice as seen in Figure 7.

There are fourteen possible point lattices called the Bravais lattices. In actuality only seven are distinct and are the basis for the seven crystal systems. The first seven Bravais lattices have points only at the corners of the lattice; the latter seven have points elsewhere in the lattice. Each of the latter have the same size,

Figure 7: Bragg reflection from a) planes and b) arrays of points.

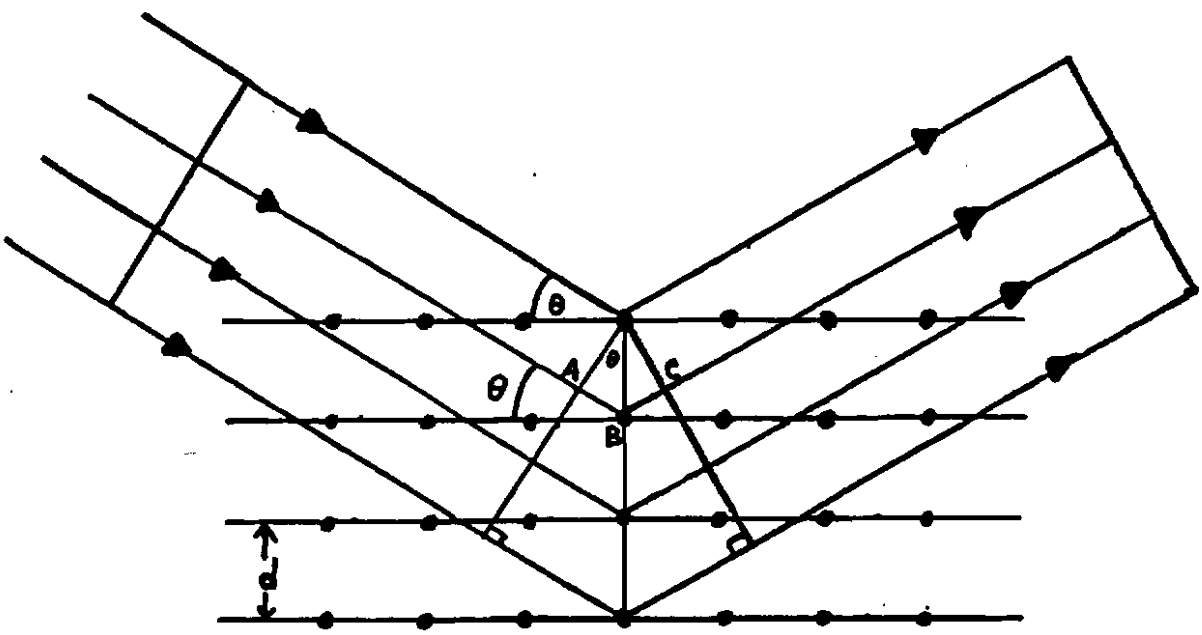
θ
θ
θ
A
C
B
d

shape, and orientation as one of the first seven, thus displaying the same conditions as the first seven.

Each point lattice has a certain inherent symmetry. Successive operations about an axis or plane will bring the lattice points back to their original positions. There are four basic operators: reflection, rotation, inversion, and rotation-inversion. All crystals belong to one of the seven crystal systems and each crystal must display a certain number of the symmetry operations characteristic of its crystal system.

Two other operators may also be at work in the crystal: a screw axis and a glide plane. Continued operation of either does not produce coincidence but does produce a pattern repeat.

When all possible combinations of the six symmetry operators are considered, the number of possible sets of points on a lattice with particular symmetry elements totals two hundred and thirty. These are called the two hundred and thirty space groups. They are listed in the International Tables for X-Ray Crystallography.[36]

A crystal is a three dimensional regularly repeating pattern of atoms. The repeating pattern is called the unit cell and can be described by a section of three dimensional space. The unit cell can be described by its lattice parameters: a, b, and c, the lattice sizes, and alpha, beta, and gamma, the angles between the axes. Planes of atoms within the crystal cross the three axis, a, b, and c, at distances x, y, and z, respectively. To avoid infinte x, y, and z values when the planes are parallel to an axis and have an infinite intercept, the reciprocals of the intercepts are taken, reduced to a common denominator and the numerator is called the Miller indices (hkl). Planes parallel to each other are of the same set and can be described by the same

Miller indices. Also, the set of planes in a crystal made equivalent by symmetry can be described by the same set of Miller indices.

The distance between planes in a set is a function of the Miller indices of the set and the lattice sizes of the unit cell. The exact relationship depends on the geometry of the crystal system. For example, in the cubic system,

$$d^2 = a^2/(h^2 + k^2 + l^2) = a^2/N \qquad (2)$$

where $N = h^2 + k^2 + l^2$. The value of d in these equations is equivalent to the d/n value of the Bragg equation.

3.2 Neutron Diffraction

Neutrons, like x-rays and electrons, have both wave and particle properties. As a neutron passes through a solid, it may be scattered by the nucleus of the atoms in the crystal in accordance with Bragg's Law.

In a reactor, neutrons are slowed down by collisions with water molecules to an average energy of 0.025 eV[37] (thermal neutrons). If the temperature is constant, the neutrons have a root mean square velocity[38] given by the equation

$$mv^2/2 = 3kT/2 \qquad (3)$$

The deBroglie wavelength can be calculated from

$$\lambda = h/mv \qquad (4)$$

Combining these equations gives

$$\lambda^2 = h^2/3mkT \qquad (5)$$

At room temperature the spectrum of wavelengths associated with these thermal neutrons becomes a Maxwellian distribution with its maximum between 1 and 2 angstroms.[39-40] These wavelengths were on the order needed to detect the d spacings of crystals.

It is necessary for constant wavelength diffraction to have a single wavelength. To produce this, the beam of neutrons passes out of the reactor and is reflected from the planes of a monochromating crystal. Only the neutrons reflected in a single direction are used to irradiate the sample.

From a powder sample the neutrons scatter in all directions off the different sets of planes in the crystal. A counter rotates around the axis of the sample in small steps, sampling portions of the scattered wave. The intensity at each angle is recorded producing a diffraction pattern.

In x-ray diffraction, the scattering occurs from the electrons. Thus the larger the atomic number, the more scattering occurs. An x-ray pattern will therefore show the positions of samarium atoms and will not detect the deuterium atoms. Neutrons, on the other hand, scatter primarily from the nucleus of an atom. Within a factor of two or three, all atoms scatter neutrons equally well.[41] Deuterium atoms can then be detected with greater ease.

The choice of deuterium rather than hydrogen is made because of the neutron capture and coherent neutron scattering crossection effects as listed in Table 2.[42]

The choice of the samarium-154 isotope was made on the basis of isotopic neutron capture crossections and availability of this isotope as shown in Table 3.

TABLE 2

CAPTURE AND COHERENT CROSSSECTIONS

FOR HYDROGEN AND DEUTERIUM

Element	Capture Crosssection (barns)	Coherent Scattering Crosssection (barns)
Hydrogen	0.332	1.76
Deuterium	0.00052	5.59

TABLE 3

ISOTOPIC ABUNDANCE, CAPTURE AND TRUE ABSORPTION

CROSSSECTIONS OF SAMARIUM

Samarium Isotope	Percent Abundance	True Absorption Crosssection (barns)	Capture Crosssection (barns)
144	3.1	-	0.72
146	2 x 10	-	-
147	15.1	-	60
148	11.3	-	4.7
149	13.9	114,000	42,000
150	7.4	3,500	104
151	-	-	1.5×10^4
152	26.6	6,350	204
154	22.6	3	51

The x-ray diffraction scattering factors vary with the Bragg angle. In neutron diffraction, the neutron scattering factor, b, does not vary significantly with angle.[43] The value of the neutron scattering factors for samarium-154 and deuterium are 0.96×10^{-24} cm and 0.667×10^{-24} cm, respectively.[44]

3.3 Calculation of Intensity[45]

The intensity of the reflections are calculated by

$$I = F^2 \; [(1 + \cos^2 2\theta)/(8\sin^2\theta\cos\theta)] \; p \; A \exp(-2B(\sin\theta/\lambda)^2 \qquad (6)$$

where p is the multiplicity of the reflection

$|F|^2$ is the geometric structure factor

$\exp(-2B(\sin\theta/\lambda)^2$ is the temperature factor

A is the absorption factor

and $[(1 + \cos^2 2\theta)/(8\sin^2\theta\cos\theta)]$ is the Lorentz-polarization factor.

3.3.1 The Geometric Structure Factor[46-47]

The amplitude and phase of a diffracted wave from a single atom is proportional to be $\exp(i\phi)$. The amplitude of the scattering is determined by the geometric structure factor, $|F|$. $|F|$ is the quantity that determines how the intensities of the reflections from the crystal depend on the atomic arrangement within the unit cell and can be calculated as a function of atomic positions, Miller indices and scattering factors of the individual atoms. F, the scattering amplitude for the unit cell, is described by

$$F = b_1\exp(i\phi_1) + b_2\exp(i\phi_2) + \ldots b_j\exp(i\phi_j) = \sum_1^j b_j\exp(i\phi_j) \qquad (7)$$

The phase difference, ϕ, between the wave scattered from an atom at coordinates x, y, z and the wave scattered from the origin (assume the origin to be 0) for the reflection with the Miller indices (hkl) is

$$\phi_j = 2\pi i\,(hx_j + ky_j + lz_j). \tag{8}$$

The equations for the wave can be rewritten as

$$\begin{aligned} F &= b_1 \exp[i2\pi i(hx_1 + ky_1 + lz_1)] \\ &+ b_2 \exp[i2\pi i(hx_2 + ky_2 + lz_2)] \\ &+ \ldots \\ &= \sum_{j=1}^{n} b_j \exp[i2\pi i\,(hx_j + ky_j + lz_j)] \end{aligned} \tag{9}$$

or

$$F_{hkl} = \sum_{j=1}^{n} b_j \exp[2i\pi i(hx_j + ky_j + lz_j)] \tag{10}$$

This can be rewritten trigonometrically as

$$\begin{aligned} F &= \sum_{n=1}^{n} b_n [\cos 2\pi i(hu_n + kv_n + lw_n) \\ &+ i\sin 2\pi i(hu_n + kv_n + lw_n)] \end{aligned} \tag{11}$$

or in the form

$$F = A + iB \tag{12}$$

where

$$A = \sum_{n=1}^{N} b_n \cos 2\pi i(hu_n + kv_n + lw_n)$$

and

$$B = \sum_{n=1}^{N} b_n \sin 2\pi i(hu_n + kv_n + lw_n).$$

3.3.2 Multiplicity[48-49]

The multiplicity factor, p, has a maximum value of 48. The actual value of p depends on the crystal form determined by the Miller indices and is equal to the number of equivalent planes in the crystal form represented by the Miller indices. For example, the (1 1 1) form represents the equivalent planes (1 1 1), (-1 -1 -1), (1 1 -1), (1 -1 -1), (-1 1 1), (1 -1 1), (-1 -1 1), and (-1 1 -1). The (1 1 1) peak represents reflections from all eight planes and the multiplicity value is therefore eight.

Tables of multiplicites can be found in Mirkin,[50] the International Tables for X-Ray Crystallography,[51] Lipson and Steeple,[52] and Cullity.[53]

3.3.3 Absorption

Neutron absorption coefficients for most materials are on the order of 0.3 cm^{-1} compared to the order of 1000 cm^{-1} for x-rays.[54] These smaller absorption coefficients make it necessary to use larger samples.[55] Reduction of intensities due to absorption is small and is normally not included in the intensity calculations unless absolute intensities rather than relative intensities are desired.

3.3.4 The Temperature Factor[56-58]

The temperature factor, B, accounts for the thermal vibration that atoms undergo about their mean positions. The amplitude of the vibrations increases with temperature and changes with the type of atom and the bonds holding it. The effect is a unit cell expansion causing the d spacing to change and thus the two theta positions to increase. The effect of this temperature factor on the intensity of the profile is

twofold: a decrease in the intensities of the lines and an increase in the intensities of the background scattering between the lines.

The temperature factor can be applied in two ways. As the overall temperature factor, it is assumed that every atom in the cell can vibrate thermally in exactly the same way. It is applied as written in Equation 6. This is normally used in the earlier stages of refinement. Later it is applied to each type of atom in the unit cell by replacing b with

$$b = b_o \exp\left[-B\ (\sin\theta/\lambda)^2\right] \tag{13}$$

The value of B is determined by use of the Wilson plot and is discussed along with the scale factor.

3.3.5 The Lorentz-Polarization Factor[59-61]

Some reflection occurs at angles that slightly deviate from the exact Bragg angle for a particular reflection, each producing some intensity. The effect on the profile is a change in height and half-width of the peak. The Lorentz factor accounts for these effects.

The equation

$$\Delta\theta = \lambda\ /(2N\sin\theta) \tag{14}$$

gives the maximum angular range of crystal rotation over which appreciable energy will be diffracted in the Bragg angle two theta. This means that the maximum height of the peak is proportional to $1/\sin\theta$. Thus the intensity is larger at lower angles and smaller at higher Bragg angles.

The changes in halfwidth in the intensity of the peak is proportional to

$$(1/\sin\theta)\ (1/\cos\theta) \text{ or } 1/\sin 2\theta \tag{15}$$

The effect is a larger width at higher two theta angles.

In powder patterns the intensity also depends on the number of crystals oriented at or near that angle. This has the form of

$$\Delta N/N = (\Delta\theta \cos\theta)/2 \tag{16}$$

Putting these three effects together the relationship becomes

$$\begin{aligned} L &= (1/\sin 2\theta)(\cos\theta)(1/\sin 2\theta) \\ &= \cos\theta/\sin^2 2\theta \qquad (17) \\ &= 1/(4 \sin^2\theta \cos\theta) \end{aligned}$$

This factor is normally constant for any given set of measurements and is not included when one is interested only in relative intensities.

X-ray beams are partially polarized and the effect is expressed as

$$P = (1 + \cos^2 2\theta)/2. \tag{18}$$

Usually the Lorentz and polarization factors are combined into a single expression:

$$LP = (1 + \cos^2 2\theta) \ / \ (8\sin^2\theta \cos\theta) \tag{19}$$

Neutron beams are not polarized and thus polarization is not included in the calculations. However, if magnetic scattering is studied, the polarization factor must be taken into account.

3.3.6 The Scale Factor[62]

It is necessary to find a way to relate the observed intensities to the absolute intensities on the same scale. This is done by use of the scale factor, k, that relates the two as

$$|F|_{abs} = k\,|F|_{rel} \tag{20}$$

The value of k can be found by use of the Wilson plot.[63] The average value of the observed intensities can be defined as

$$\overline{I}_{rel} = (\,|F|^2_{rel}\,)avg \tag{21}$$

For a unit cell containing N atoms it can be shown that the theoretical average intensity is given by

$$\overline{I}_{abs} = \sum_{i=1}^{N} f_i^2 \tag{22}$$

Ideally, the ratio

$$\overline{I}_{abs}/\overline{I}_{rel} = \Sigma_i f_i^2 / \,(|F|^2)avg \tag{23}$$

should be the scaling factor required to place the individual intensities on an absolute scale. However, thermal vibrations directly affect the atomic positions in the real crystal. For each atom, then, the equation becomes

$$\overline{I}_{abs} = \sum_{i=1}^{N} f_{io}^2 \exp(-2B(\sin\theta/\lambda)^2) \tag{24}$$

If the temperature factor, B, has the same value for all atoms then

$$\overline{I}_{abs} = \exp(-2B(\sin\theta/\lambda)^2) \sum_{i=1}^{N} f_{oi}^2 \tag{25}$$

Now, if

$$C = \bar{I}_{rel} / \bar{I}_{abs} \tag{26}$$

then

$$\bar{I}_{rel} = C \exp(-2B(\sin\theta/\lambda)^2) \sum_{i=1}^{N} f_{oi}^2 \tag{27}$$

and

$$\bar{I}_{rel} / \sum_{i=1}^{N} f_{oi}^2 = C \exp(-2B(\sin\theta/\lambda)^2). \tag{28}$$

Taking the ln of both sides results in

$$\ln \frac{\bar{I}_{rel}}{\sum_{i=1}^{N} f_{oi}^2} = \ln C - 2B(\sin\theta/\lambda)^2 \tag{29}$$

If the left side is plotted against $(\sin\theta/\lambda)^2$, the result is a straight line with intercept ln C and a slope of -2B (from which the temperature factor can be calculated). C is related to the k of Equation 20 by

$$k = C^{-\frac{1}{2}} \tag{30}$$

3.4 Profile Analysis[64-65]

The analysis of raw data begins by determining the two theta values of the observed reflections. Sin θ and/or $\sin^2\theta$ values are then calculated.

If the lattice parameters are known, the appropriate d spacing equation combined with Bragg's law, can be used to calculate the sin θ and/or $\sin^2\theta$ values. A comparison of the calculated and observed sin θ or $\sin^2\theta$ values is made. A matching set determines the characteristic set of N values and thus confirms the validity of the crystal system.

A copy of the characteristc N values for several crystal systems is reproduced from Lipson and Steeple[66] in Appendix A. A more complete list can be found in Mirkin.[67]

If a match is not achieved, another crystal system is chosen and the procedure repeated until a match is achieved.

For the cubic system, the appropriate equation to be used is

$$\lambda^2/4a^2 = (\sin^2\theta)/N \tag{31}$$

where $N = h^2 + k^2 + l^2$.

In the hexagonal case, the equation is

$$\lambda^2/(4\sin^2\theta) = 4N / 3a^2 + l^2 /c^2 \tag{32}$$

where $N = h^2 + hk + k^2$. During initial indexing in the hexagonal case, only reflections with $l = 0$ are considered. If these values match, the calculated values of $\sin^2\theta$ can then be adjusted for different values of l and a more extensive comparison made.

If the lattice parameters are unknown, the integers, N, are determined by finding the common factor in the $\sin^2\theta$ values either by trial and error or by difference methods. The multiples of the common factor then correspond to the N values and are then matched to the characteristic set of N representing the crystal systems. High two theta angles should be used for determining the lattice parameters using the appropriate d spacing equation. Since there are two lattice parameters, the lattice parameters are determined by solving simultaneous equations for two peaks. More complete descriptions of these methods can be found in Lipson and Steeple,[68] Mirkin,[69] and Cullity.[70]

The more unknown parameters there are, the more difficult it becomes to index the pattern. Several graphical methods have been developed to help solve the more complex problems. Hull-Davey[71-72] took the logs of the plane spacing equations and after rearranging them and incorporating the c/a ratio into the equation, he subtracted the equations for two different plane spacings. The resultant equation depends only on h, k, l and the c/a ratio. By solving these two equations simultaneously for different c/a values, a graph is obtained suitable for indexing any pattern.

To use the graph, log d values or the d spacings of the pattern are calculated and marked on a piece of paper using the scale of the graph. The strip is placed on the chart and moved around to find a c/a ratio that matches. The (hkl) indices are then read from the curves. Any systematic absence and peaks containing more than one reflection can be determined. This furthur helps identify the space group to which the structure belongs.

The lattice sizes are then determined by solving simultaneous equations for the high angle reflections.

Bunn,[73] Schwartz and Summa,[74] Harrington,[75] and Bjurstrom[76] are also credited with graphical methods that work in the same way as a Hull-Davey chart. Graphs for each crystal system can be found in Mirkin.[77]

The next step involves the determination of the number of atoms in the unit cell.[78] The equation

$$A = V' / \rho 1.66042 = nM \qquad (33)$$

here V' is the volume in cubic angstroms and rho the density in g/cc, the molecular weight of the molecule, A the sum of all the atomic weights in the unit cell, and n is the number of molecules in the unit cell. The number of atoms per unit cell is then calculated from n.

The space group and atomic positions of the atoms must then be determined by trial and error.[79] The presence or absence of some Miller indices eliminates some space groups. The pattern of relative intensities can be compared to already existing patterns in Mirkin[80] and the choice of a space group can be made. Mirkin[81] also contains lists of compounds and their structures. The space group of a similar compound can be applied to a substance. Mirkin[82] also provides a table indexing space groups and coordinates using the number of atoms in the unit cell.

Once a space group is chosen, the corresponding symmetry operators are located in the International Tables for X-Ray Crystallography.[83] Numbers are chosen for the atomic positions and inserted into the general coordinates of the space group. The structure factors and the intensities are determined at each angle. This calculated pattern is then compared to the observed pattern. Adjustments can then be made on any or all parameters (including positions and lattice sizes) and the pattern is refined until the best fit is obtained.

The refinement process[84-86] was also trial and error and it is made easier by use of the computer. Each facility has its own programs, but most are based on the weighted least squares program formulated by R.M. Rietveld.[87] A description of the least squares analysis is given in Appendix C.

Reliability factors or R factors[88] are normally used to determine the goodness of fit between the experimental and calculated diffraction profiles. Several R values are defined by Rietveld and Wilson and are discussed in Stout and Jensen. Most R values are variations of one of two basic forms:

$$R = \frac{\Sigma|\Delta F|}{\Sigma|F_o|} = \frac{\Sigma\big||F_o| - |F_c|\big|}{\Sigma|F_o|} \tag{34}$$

or

$$R = \frac{\Sigma_i W_i \left(|F_{oi}| - |F_{ci}|\right)^2}{\Sigma_i W_i |F_{oi}|^2} \tag{35}$$

SECTION 4

EXPERIMENTAL

4.1 The Hydriding Apparatus

The stoichiometries of the samarium hydrides prepared were determined using the pressure-temperature-volume relationship of the ideal gas law. Careful measurements of pressure, volume, and temperature of the gas, and the mass of the samarium are needed. A schematic of the hydriding apparatus used to prepare the samples is shown in Figure 8.

The volume of the system was determined by taking a standard, known volume, and measuring its temperature and pressure after filling it with deuterium. The rest of the system was then closed off and evacuated. The standard volume was then opened, flooding the system. When equilibrium was re-established, the temperature and pressure of the system were measured and the volume calculated using the ideal gas law. The volume of the system was 16.16 liters and includes the hashed lines, the standard volume, the ballast tank and the quartz tube.

Temperatures were determined using chromel-alumel thermocouples. The temperature of the reaction vessel (quartz tube) was measured by placing the thermocouple in the bottom end of the quartz sample holder against the reaction vessel. The gas temperature in the manifold was measured by a thermocouple placed on the copper line leading to the quartz tube. Temperatures inside the quartz tube were much hotter than the temperature of the gas in the manifold, but because the quartz tube

Figure 8: The hydriding apparatus for preparation of samarium deuteride. 1. Standard volume 2. Raw deuterium 3. Hastings Vacuum gauge 4. Baratron pressure manometer 5. Ballast tank 6. Temperature readout 7. Temperature controller 8. Lindberg tube furnace 9. Quartz tube 10. Uranium bed 11. Diffusion (Veeco) pump with Phillips-Granville Ionization gauges.

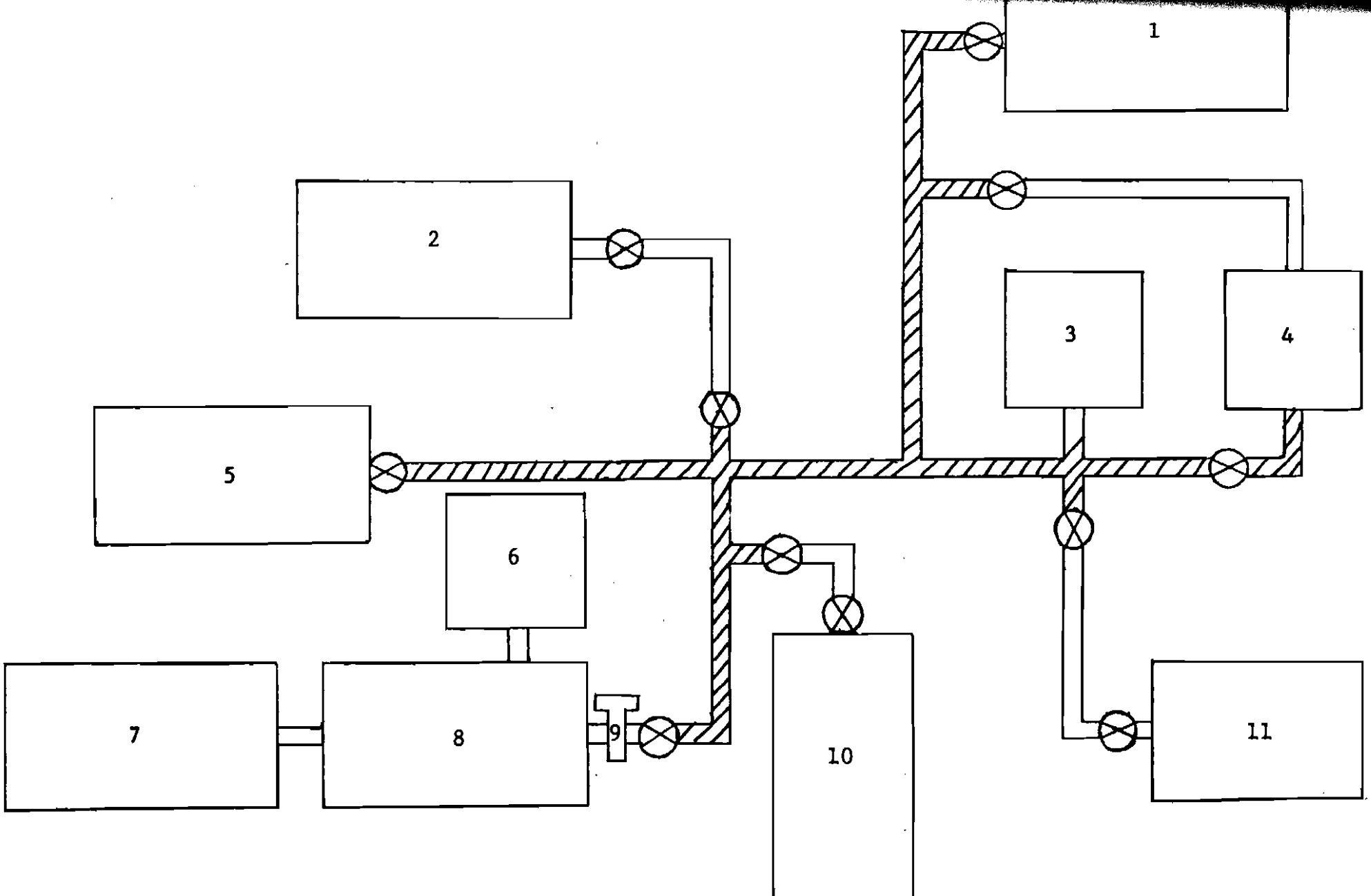
1
2
3
4
5
6
7
8
9
10
11

has a volume (0.04 liters) that was negligible when compared to the volume of the entire system, the gas temperature was recorded as the reaction temperature.

Pressure was measured by means of an MKS model 170M baratron capacitance manometer.

4.2 The Diffraction Apparatus

A schematic of the Omega West Diffractiometer at the Los Alamos National Laboratory is shown in Figure 9. A copper crystal set to reflect from its (220) planes is used as a monochromator. The six foot cylindrical shield around this crystal was filled with iron fillings and oil and lined with uranium. The shield was capable of rotating in order to change the beam direction from the reactor and the wavelength of the neutrons, but was normally left in a fixed position. The specimen table rotated independently. The counter contained gaseous boron trifluoride and revolved around the axis of the specimen table by tenths of a degree. The neutrons enter the counter and react with the boron-10 isotope according to the reaction:

$$ {}^{10}_{5}B + {}^{1}_{0}n = {}^{7}_{3}Li + {}^{4}_{2}He + 2.8 \text{ MeV} \qquad (36) $$

The lithium and helium nuclei produce on the average 7×10^4 ion pairs.[89] The electrons are accelerated to the anode producing a current that can be recorded as a count. Additional electrons are produced by the collisions of the ion pairs with the gas molecules but these usually measure less than one percent of the total.[90]

Figure 9: A schematic of the Omega West Diffractometer.
1. Control and Recording System 2. Reactor
3. Shield 4. Monochromating Crystal
5. Specimen Table 6. Boron Trifluoride Counter

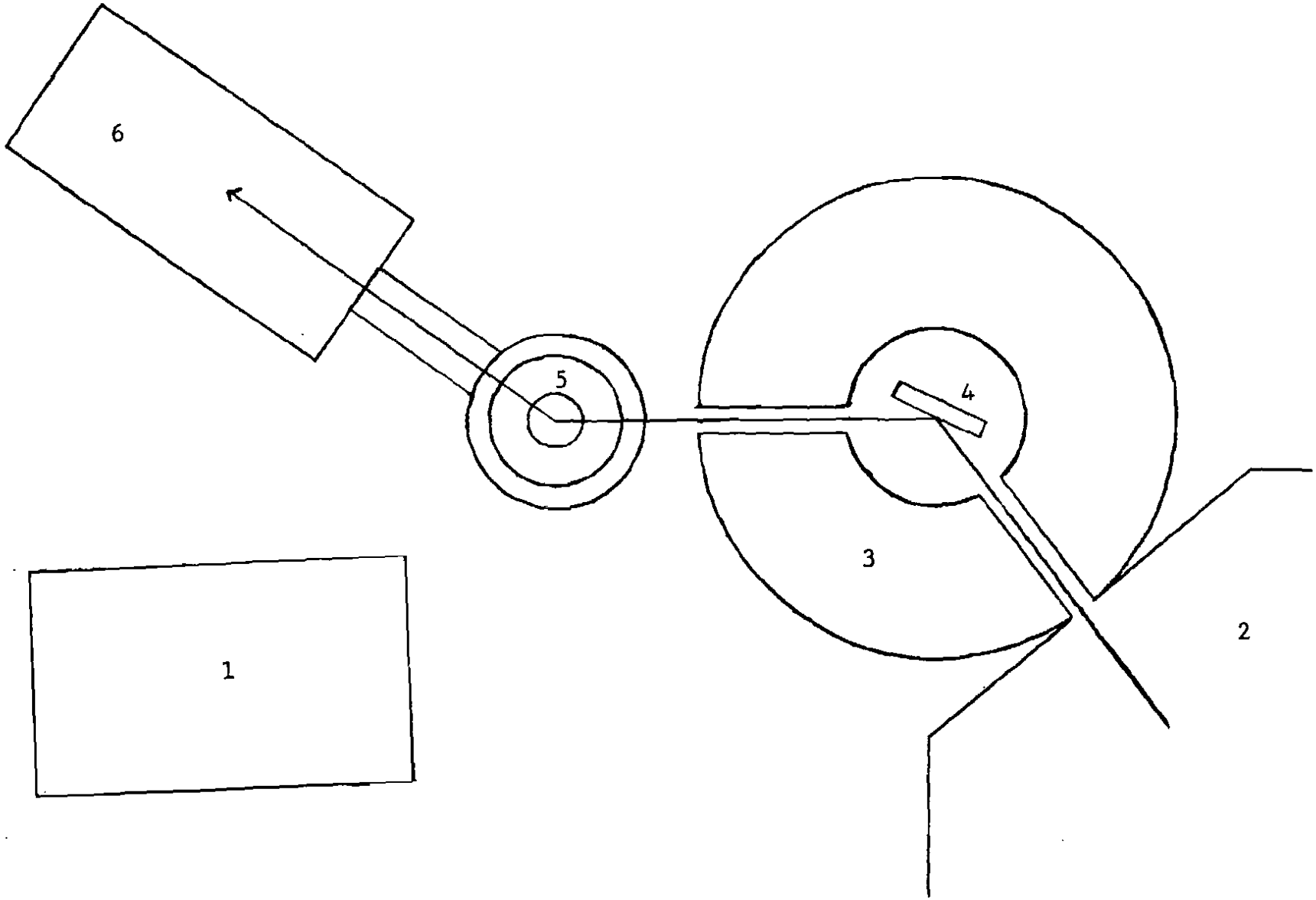
6
5
4
3
2
1

4.3 Wavelength Determination

The wavelength of the diffracted beam was determined by diffraction from a niobium oxide standard. The wavelengths were determined for each reflection in the profile. A weighted average was calculated by multiplying the peak wavelength by its intensity and averaging these. The wavelength thus determined was 1.275 angstroms.

4.4 Deuterium Reagent

Impurities in the deuterium can produce surface reactions that inhibit the hydriding of the samarium metal. A uranium bed was designed and used to reduce this possibility and to purify the deuterium. Uranium and deuterium were allowed to react. As necessary, the uranium hydride was heated, driving off the deuterium and leaving the unwanted uranium compounds behind.

4.5 Samarium Reagent

The samarium-154 isotope was separated from the raw metal on the Calutron at the Oak Ridge National Laboratory. To protect it from impurities, it was loaded into a glass container, evacuated, sealed and placed in a second can, and again evacuated and sealed. Analysis shows the samarium to be 98.69% samarium-154. The detailed analysis of the sample is recorded in Appendix E. Since samarium is very sensitive to contamination, it was opened and prepared for use under an inert argon atmosphere. A continual influx of welding grade argon flowed into a glove box. By mass spectrographic analysis, the oxygen level in the box was determined to be less than 0.1% oxygen after a minimum flushing time of two hours.

The sample was sawed, using kerosene as a lubricant, into slices and then cut into small pieces, washed twice with anhydrous ethanol and loaded into a quartz tube that had previously been cleaned, outgassed at 450 C, and carefully weighed. The tube was then placed on the system for hydriding.

4.6 Samarium Deuteride Preparation

When the system was evacuated to a base pressure of 2×10^{-7} torr deuterium from the uranium bed was allowed to fill the system to a pressure between 700-1000 torr. The initial temperature of the quartz tube and the gas were recorded. The stopcock was opened and the temperatures and pressure were again recorded. Reaction usually started immediately and proceeded very quickly with an exothermic heat of reaction. It was impossible to record these temperatures due to the rapid rate of the increase, although maximums were recorded. Once the reaction slowed and the tube started to cool the temperature was adjusted to $250 \pm 5^{o}C$. Reaction was allowed to proceed in most cases over days and sometimes weeks until equilibrium was established. The temperature was then lowered or raised and equilibrium was re-established at each new temperature. In cases where the higher stoichiometries were made, the tube was then allowed to take on more hydrogen as the tube was allowed to cool to room temperature.

Due to the limited amount of samarium-154 isotope available, the $SmD_{2.89}$ and $SmD_{2.99}$ samples were made as previously described. The $SmD_{2.38}$ and $SmD_{1.97}$ samples were prepared by dissociation of one of the previous samples. The $SmD_{2.89}$ sample was placed on the evacuated system and opened to the system. The temperature was increased. Dissociation occurs in the manner shown in Figure 5. As a H/M ratio of 1.8 is

approached, the equilibrium pressures are small. This necessitated the removal of deuterium in successive steps until a stoichiometry of $SmD_{1.97}$ was reached. After dissociation was performed, this same sample was again placed on the system and opened to a measured pressure of deuterium. The association process was halted at a stoichiometry of $SmD_{2.38}$. Table 4 provides the information used to calculate the stoichiometry of the samples.

4.7 The Diffraction Procedure

The quartz tube shown in Figure 10 containing the sample was placed in an aluminum cyclinder pictured in Figure 11. The cylinder was then evacuated and placed on the specimen table of the diffractometer. A diffraction pattern for two theta values ranging from 2 to 90 degrees was performed.

The raw data was indexed by hand and computer to determine the crystal structure and lattice sizes indicated by the data. This was then fed into the program CWPREF which indexed the experimental data and prepared the experimental diffraction profile. A data file containing the proposed space group information was then created and fed into the program CWLS. This program calculated a profile and then compared it with the experimental profile produced in CWPREF. The calculated profile was then refined in steps by changing the CWLS parameters until a best fit was obtained.

R values were used to determine the extent of the best fit between the experimental and calculated patterns. Three R factors were used in this analysis:

TABLE 4

STOICHIOMETRIC DETERMINATION

Sample No.	Grams Sm	Moles Sm	Pressure Difference*	H/M Ratio	Tube No.
1	15.797	0.1026	171.93	2.89	86
2	18.681	0.1213	210.40	2.99	75
3	15.797	0.1026	112.69	1.97	86
4	15.797	0.1026	136.61	2.38	86

* Pressures in torr

Volume = 16.16 liters

Temperature = 27.2°C

Figure 10: The quartz tube used as the reaction vessel for samarium-deuteride preparation.

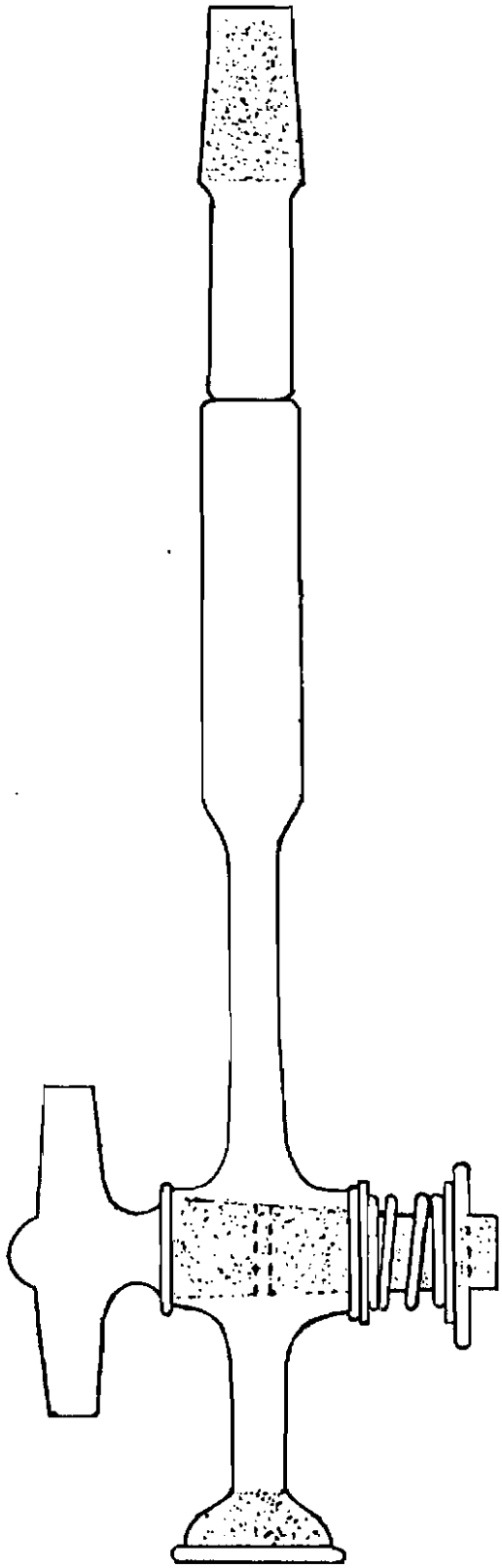

Figure 11: The aluminum cyclinder used to hold the samarium deuteride during neutron diffraction.

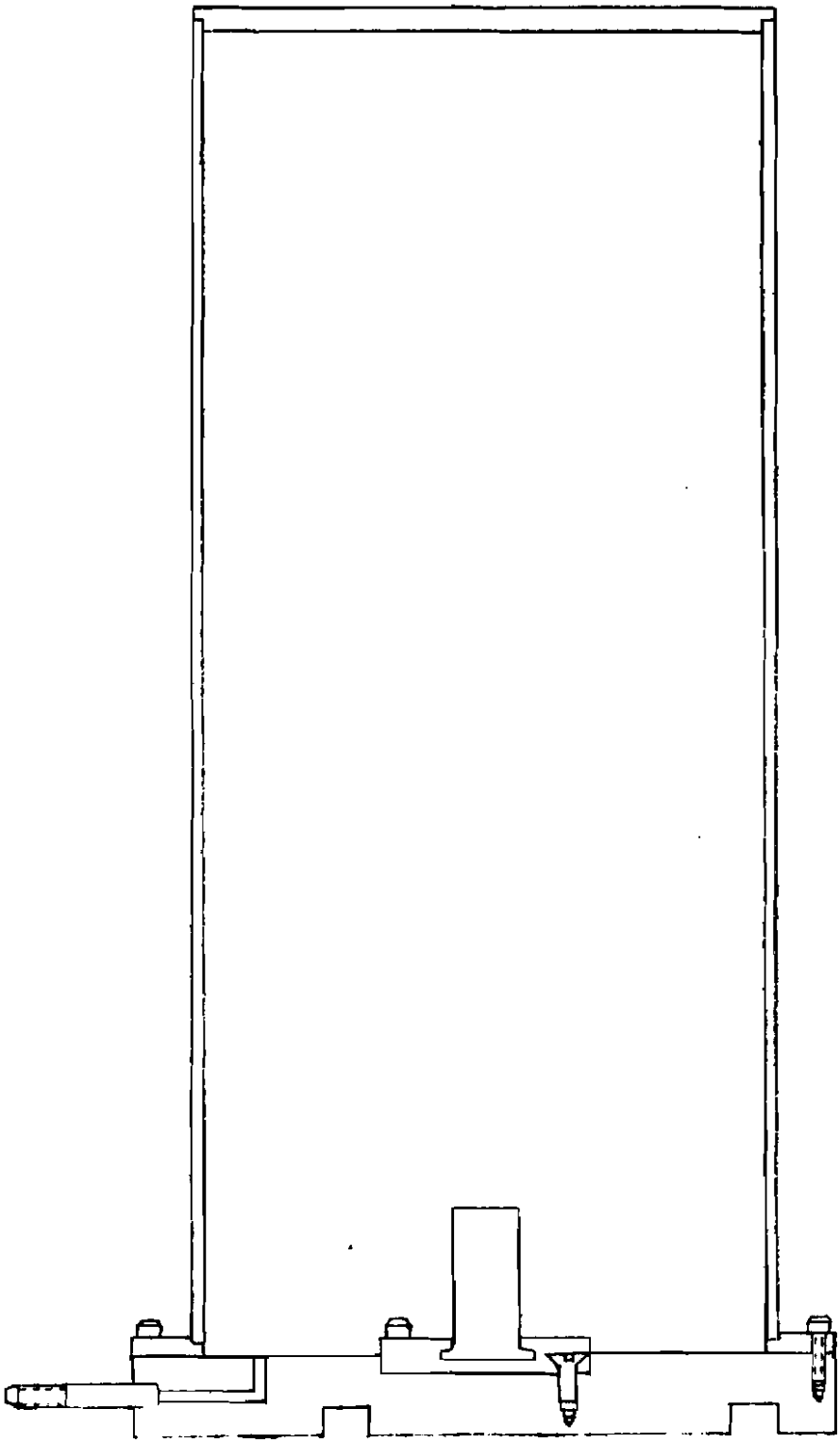

$$R\ \text{profile} = \frac{100 \sum \left| F_{obs} - F_{calc}S \right|^2}{\sum \left| F_{obs} \right|} \qquad (37)$$

$$R\ \text{weighted} = \frac{100 \left[\sum w \left(\left| F_{obs} - F_{calc}S \right| \right)^2 \right]^{\frac{1}{2}}}{\left[\sum w \left| F_{obs} \right|^2 \right]} \qquad (38)$$

and

$$R\ \text{expected} = \frac{100 \left[\text{no. of degrees of freedom} \right]^{\frac{1}{2}}}{\sum w \left| F_{obs} \right|^2} \qquad (39)$$

Standard deviations for the refined parameters were calculated during the refinement as outlined in Appendix D.

SECTION 5

DATA AND RESULTS

The raw data for each sample appears in Appendix F. The experimental profiles are shown in Figures 12-15. $SmD_{1.97}$ and $SmD_{2.38}$ are both face centered cubic. $SmD_{2.99}$ is hexagonal. $SmD_{2.89}$ contains both the cubic and hexagonal phases.

5.1 The Cubic Analysis

The proposed cubic space group for samarium hydride is F 4/m 3 2/m or O_h^5 (see Appendix G) with

3 Sm at 0 ½ ½

1 Sm at 0 0 0

8 D at ¼ ¼ ¼

and 4 D at 0 ½ 0.

Calculations by hand and by computer analysis using CWPREF, CWLS, and CWPLOT (Appendix B) confirm this is the correct structure. The refined profiles for the cubic samarium deuterides are shown in Figures 16-18. Cubic positions determined in this study are listed in Table 5. The determined lattice sizes are listed in Table 6. A comparison of experimental and calculated intensities are listed in Figures 19-21.

5.2 The Hexagonal Analysis

The peaks were indexed both by hand and by use of the CWPREF program. Table 7 compares the two sets of calculations. Peaks numbered

7, 13, 17, 22, and 24 were found to match the hexagonal N pattern A, 4A, 7A, 9A, 12A, and 13A where $A = \lambda^2/3a^2$. The lattice parameter, a, is determined to be 3.7638 A. The log d values were calculated and plotted along the scale on a Schwartz and Summa graph[91] for indexing hexagonal crystals. A match was made along the line representing the c/a ratio of 1.79. Each line was indexed accordingly. The (0 0 1) lines are either absent or too weak to observe.

The relative intensities of these peaks were compared to those of known hexagonal structures in Mirkin.[92] An approximate match is made for H15 structure representing K_3Bi and Na_3As. The structure correlates with the P $6_3/m\ m\ c$ or D_{6h}^4 space group (see Appendix G) with these coordinates:

2 Sm at 1/3 2/3 ¼

2 D at 0 0 ¼

4 D at 1/3 2/3 z and

2/3 1/3 z+½

where z = 0.583. This information was used in the CWLS program to refine the calculated hexagonal profile. The best fit between the experimental and calculated profiles is shown in Figures 22-23 for $SmD_{2.89}$ and $SmD_{2.99}$. The refined coordinates and parameters are shown in Table 8 for both samples. A comparison of the experimental and calculated intensities is shown in Figure 24-25. The lattice sizes are listed in Table 6. R values for both refinements are shown in Table 9.

Figure 12: Raw neutron diffraction profile for $SmD_{1.97}$

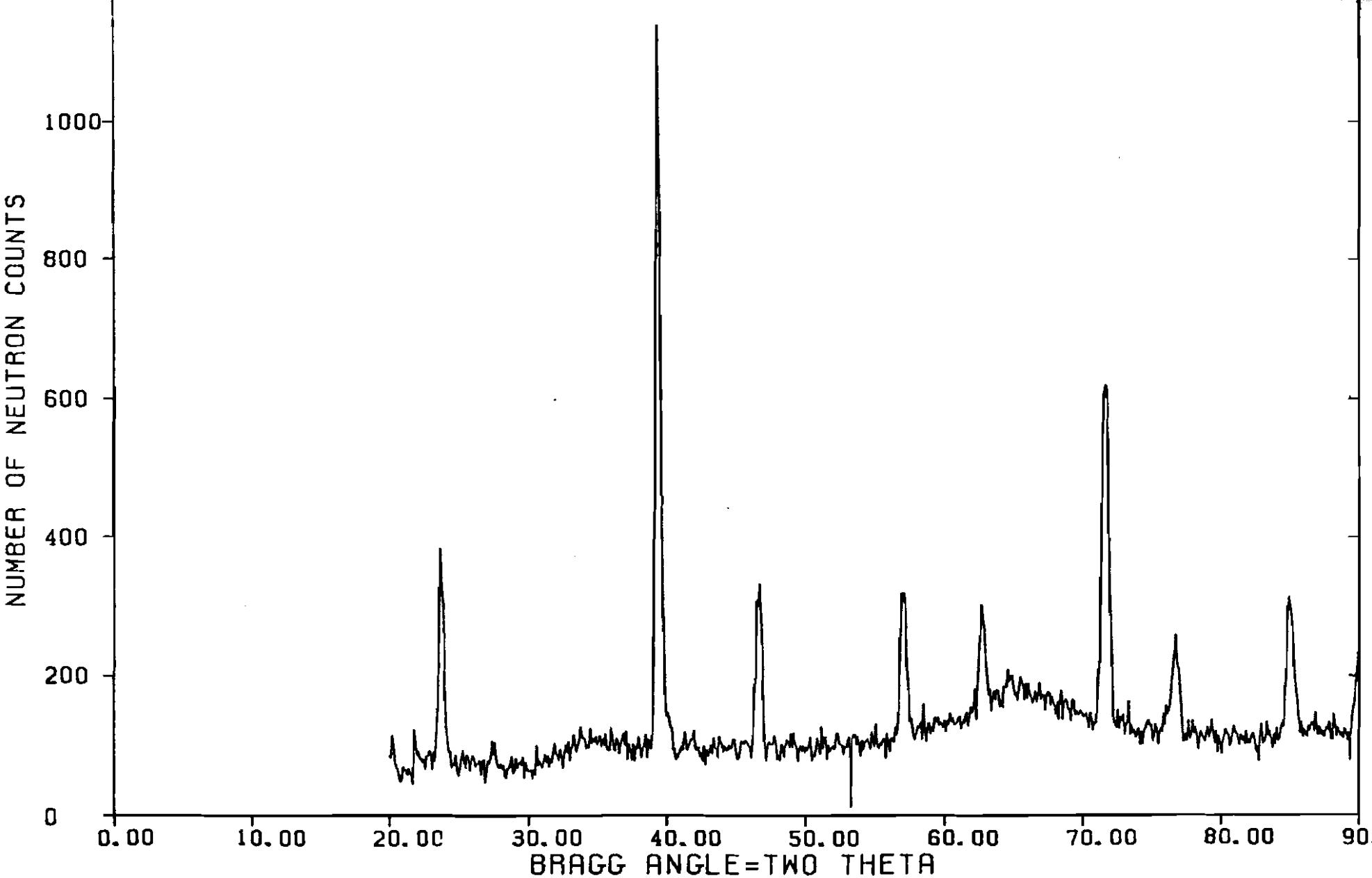
NUMBER OF NEUTRON COUNTS
0
200
400
600
800
1000
0.00
10.00
20.00
30.00
40.00
50.00
60.00
70.00
80.00
90.
BRAGG ANGLE=TWO THETA

Figure 13: Raw neutron diffraction data profile for $SmD_{2.38}$

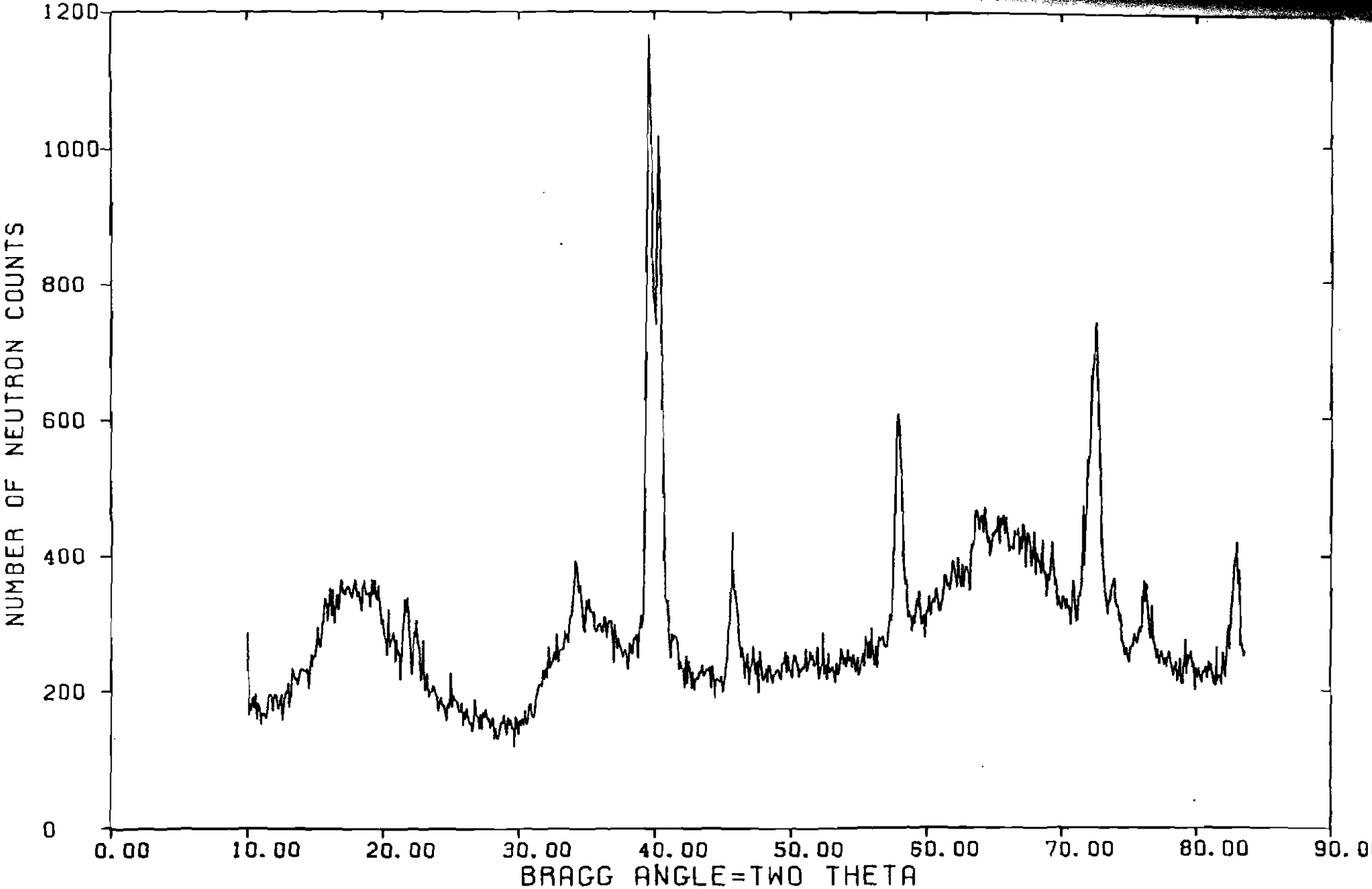
NUMBER OF NEUTRON COUNTS
1200
1000
800
600
400
200
0
0.00
10.00
20.00
30.00
40.00
50.00
60.00
70.00
80.00
90.0
BRAGG ANGLE=TWO THETA

Figure 14: Raw neutron diffraction profile for $SmD_{2.89}$

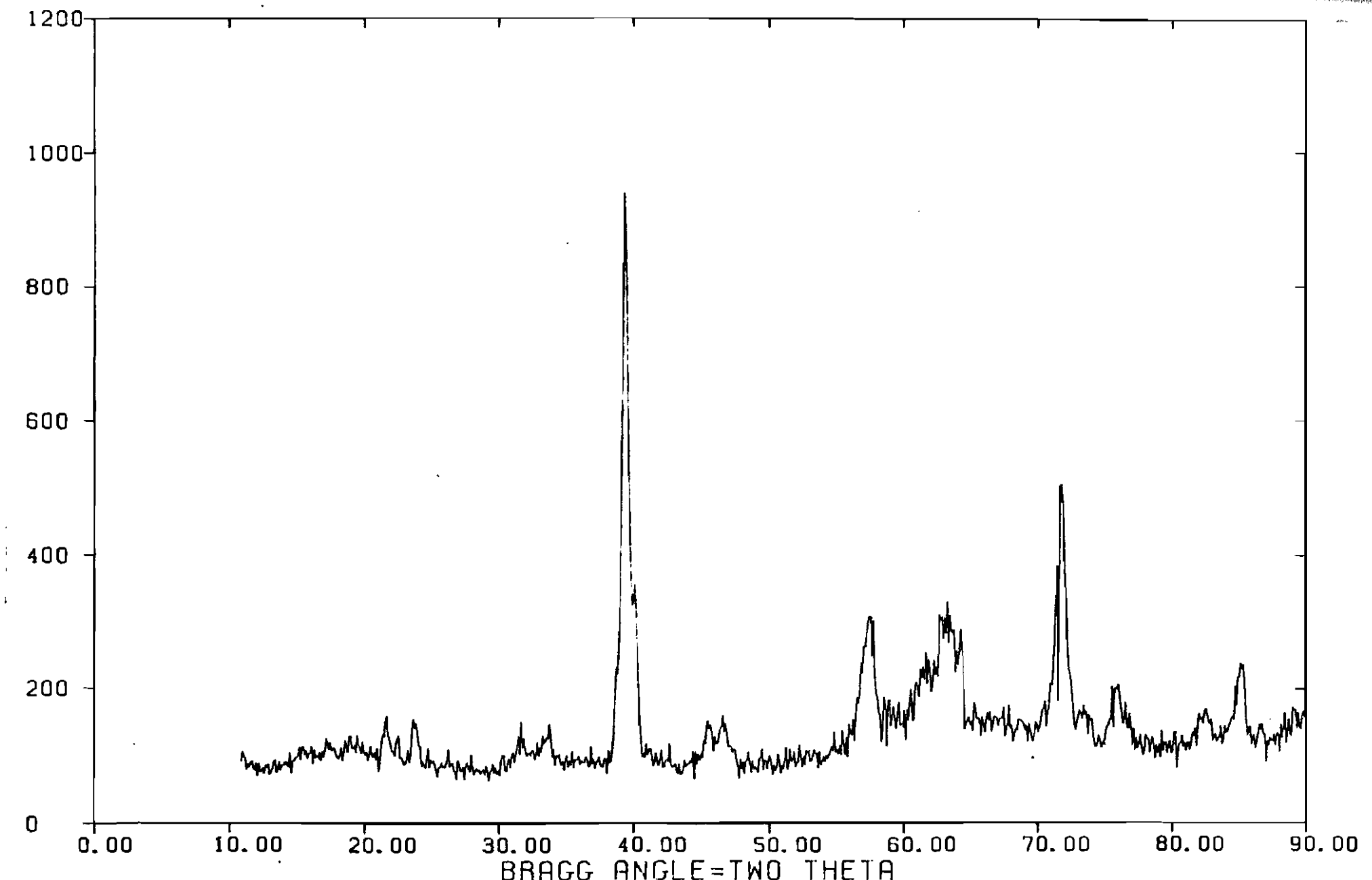
1200
1000
800
600
400
200
0
0.00
10.00
20.00
30.00
40.00
50.00
60.00
70.00
80.00
90.00
BRAGG ANGLE=TWO THETA

Figure 15: Raw neutron diffraction profile for $SmD_{2.99}$

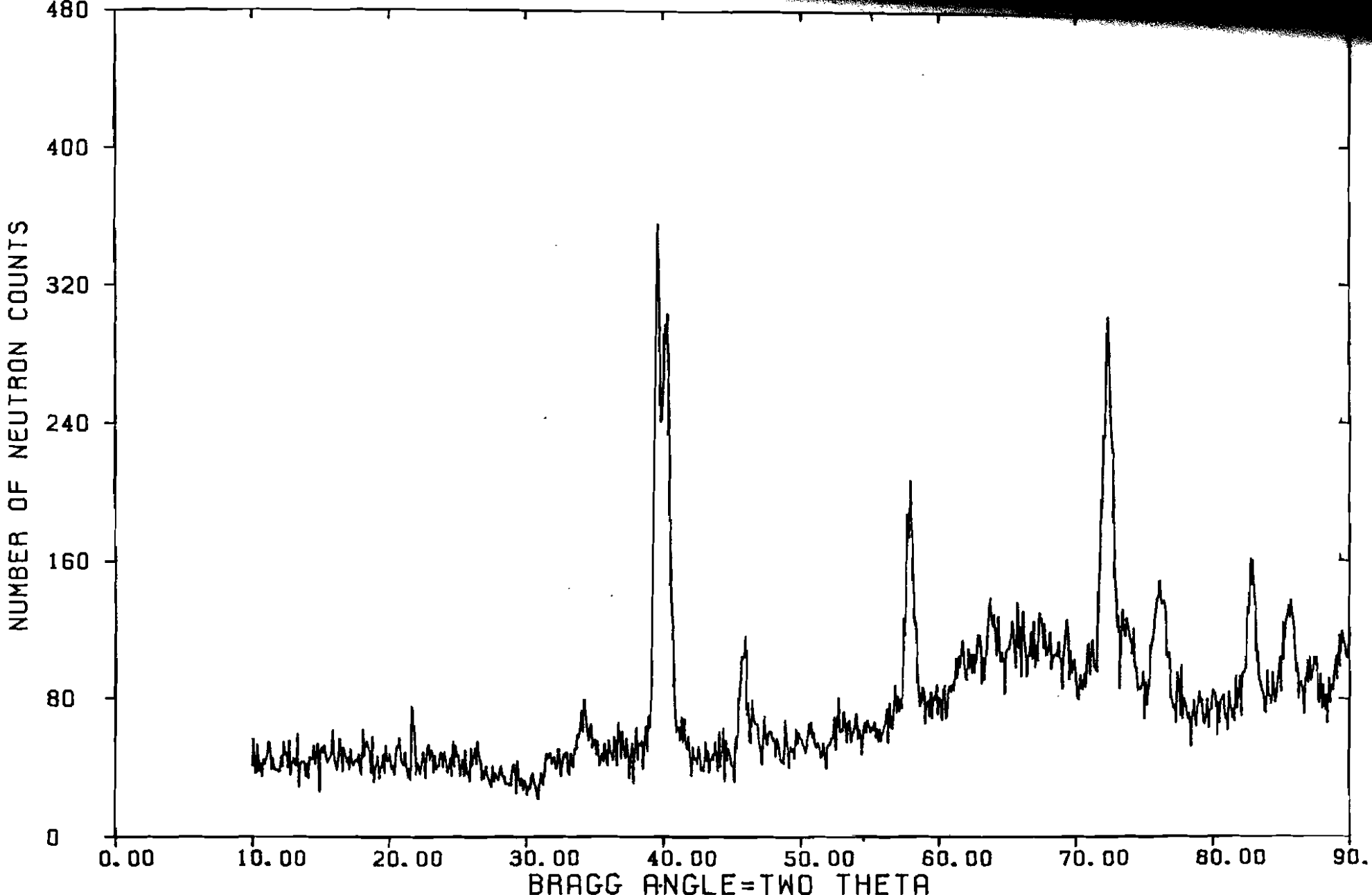
NUMBER OF NEUTRON COUNTS
480
400
320
240
160
80
0
0.00
10.00
20.00
30.00
40.00
50.00
60.00
70.00
80.00
90.
BRAGG ANGLE=TWO THETA

Figure 16: Comparison of the experimental and refined profiles for cubic $SmD_{1.97}$

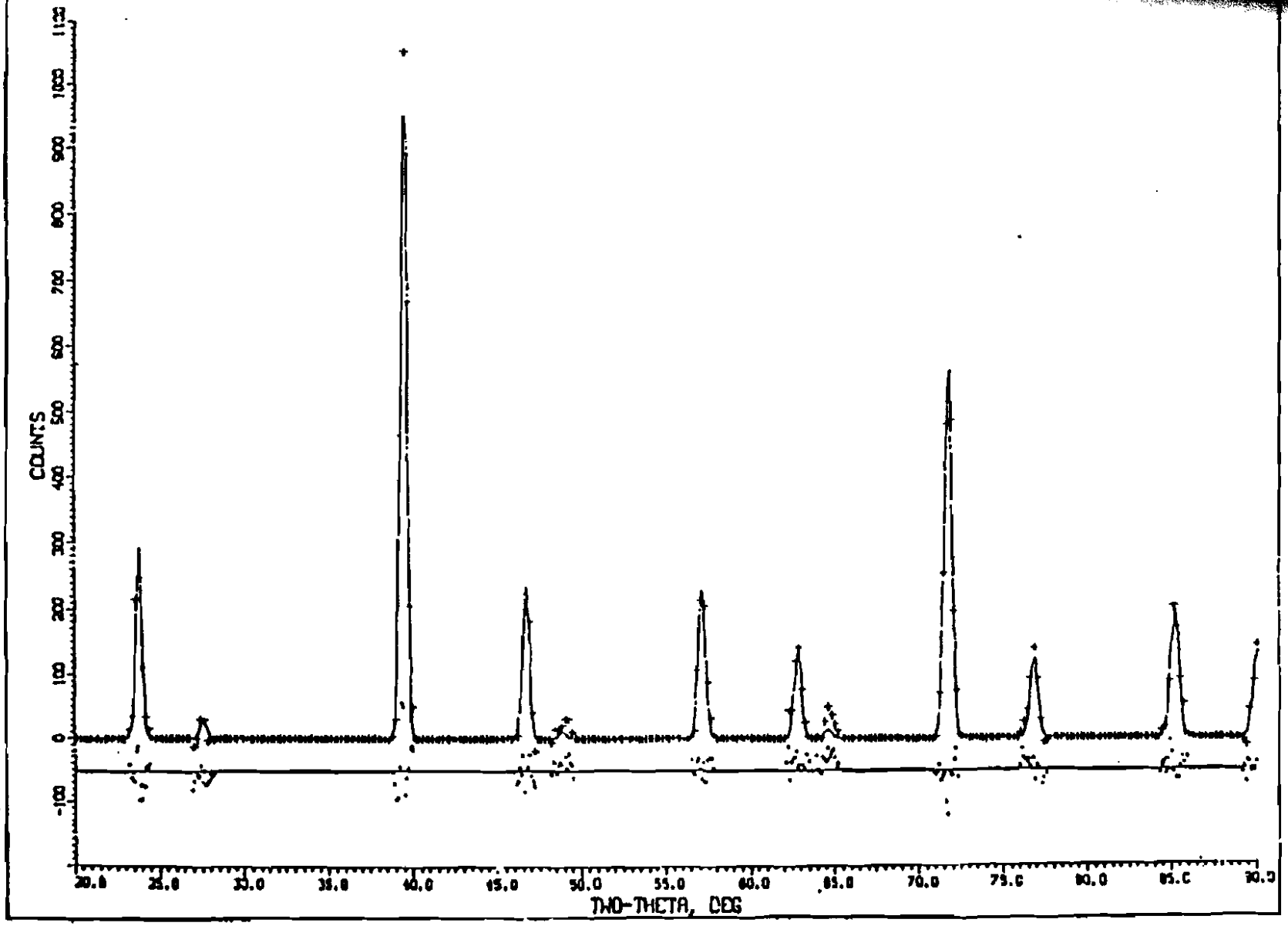
COUNTS
TWO-THETA, DEG

Figure 17: Comparison of the experimental and refined profiles of cubic $SmD_{2.38}$

SMD 2.38

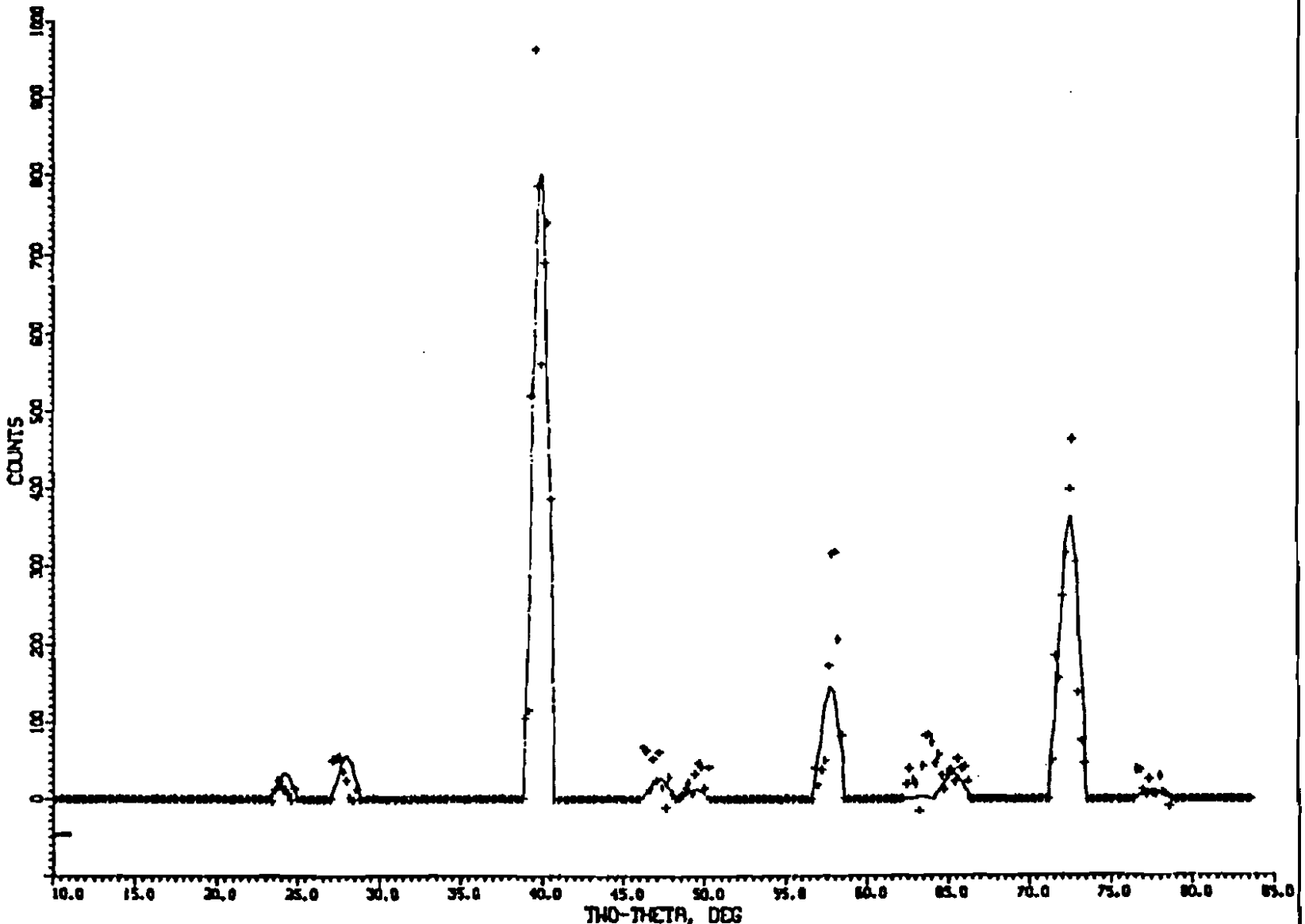
COUNTS
0
100
200
300
400
500
600
700
800
900
1000
10.0
15.0
20.0
25.0
30.0
35.0
40.0
45.0
50.0
55.0
60.0
65.0
70.0
75.0
80.0
85.0
TWO-THETA, DEG

Figure 18: Comparison of the experimental and refined profiles of the cubic $SmD_{2.89}$

SMD 2.89 CUBIC

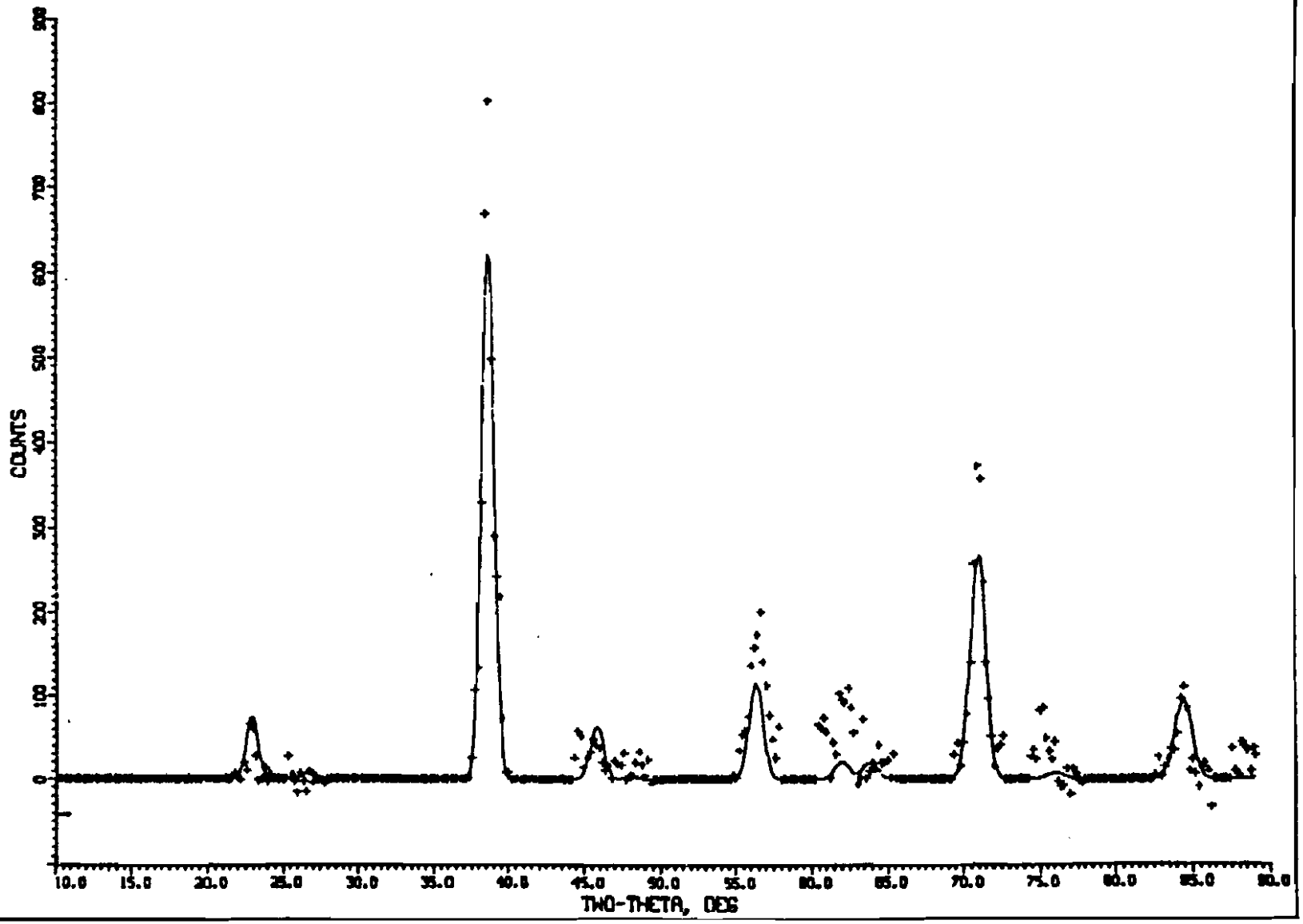

TABLE 5

ATOMIC POSITIONS IN THE CUBIC SAMARIUM DEUTERIDES

Cubic		x	y	z	N	N_1
1.97	1 Sm	0	0	0	0.04355 ± 0.00339	1.04520
	3 Sm	0	½	½	0.12689 ± 0.00339	1.01512
	8 D	¼	¼	¼	0.35268 ± 0.00339	1.05805
	4 D	½	0	0	0.00000 ± 0.00339	0.00000
2.38	1 Sm	0	0	0	0.04071 ± 0.00602	0.97704
	3 Sm	0	½	½	0.15411 ± 0.00602	1.23288
	8 D	¼	¼	¼	0.33287 ± 0.00602	0.99862
	4 D	½	0	0	0.16656 ± 0.00602	0.99932
2.89	1 Sm	0	0	0	0.00889 ± 0.00280	0.21336
	3 Sm	0	½	½	0.12229 ± 0.00280	0.97832
	8 D	¼	¼	¼	0.30105 ± 0.00280	0.90316
	4 D	½	0	0	0.15069 ± 0.00280	0.90423

N_1 represents the ratio; calculated site occupation factor/expected site occupation factor. The ratio should = 1 if the site is filled as expected for the structure.

TABLE 6

LATTICE SIZES OF EXPERIMENTAL SAMARIUM DEUTERIDES

H/M	a	c
1.97	5.3274 ± 0.0008	-
2.38	5.2975 ± 0.0059	-
2.89cub	5.3215 ± 0.0042	-
2.89hex	3.7600 ± 0.0156	6.7874 ± 0.0156
2.99	3.7493 ± 0.0038	6.7212 ± 0.0045

a and c in Angstroms

Figure 19: Comparison of the cubic intensities of $SmD_{1.97}$
POSN is the 2θ angle,
INUC is the calculated intensity, and
IOBS is the observed intensity.
ESD is the estimated standard deviation.

H	K	L	POSN	INUC	IOBS	ESD
1	1	1	2378	1398	1329	49
2	0	0	2756	132	0	0
2	2	0	3944	4664	4890	79
3	1	1	4664	1180	1126	50
2	2	2	4886	48	165	37
4	0	0	5708	1171	1257	53
3	3	1	6277	715	905	55
4	2	0	6460	69	301	51
4	2	2	7158	3174	3049	71
5	1	1	7680	535	598	40
3	3	3	7680	178	199	13
4	4	0	8512	1230	1336	57
5	3	1	9005	893	918	76

Figure 20: Comparison of the cubic intensities of $SmD_{2.38}$

H	K	L	POSN	INUC	IOBS	ESD
1	1	1	2422	364	192	61
2	0	0	2802	629	473	54
2	2	0	3997	9565	10313	124
3	1	1	4722	330	632	72
2	2	2	4945	150	382	70
4	0	0	5773	1934	2747	94
3	3	1	6347	13	802	93
4	2	0	6531	464	902	102
4	2	2	7245	5311	5016	111
5	1	1	7761	127	370	60
3	3	3	7761	42	123	20

Figure 21: Comparison of the cubic intensities of $SmD_{2.89}$

H	K	L	POSN	INUC	IOBS	ESD
1	1	1	2386	716	482	54
2	0	0	2763	71	32	48
2	2	0	3953	6450	6958	97
3	1	1	4674	687	828	58
2	2	2	4896	32	305	46
4	0	0	5719	1328	2761	78
3	3	1	6289	245	1397	79
4	2	0	6472	238	525	67
4	2	2	7181	3379	3808	90
5	1	1	7694	71	684	54
3	3	3	7694	24	228	18
4	4	0	8528	1335	1201	77
5	3	1	9022	15	959	134
6	0	0	9187	74	2140	619
4	4	2	9187	295	8560	2478

TABLE 7

INDEXING HEXAGONAL SMD

$2\theta_{exp}$	$2\theta_{cal}$	$\sin^2\theta_{exp}$	$\sin^2\theta_{calc}$	$d_{avg.}$	hkl	reflection
	25.00		.0468		101	1
	31.70		.0746		102	2
	39.60	.1153	.1147	1.879	110	3
40.40	40.80	.1192	.1215	1.847	103	4
	41.20		.1238		111	5
	45.90				112	6
46.00	46.10	.1527	.1533	1.633	200	7
47.40	47.60	.1616	.1628	1.587	201	8
50.80	51.20	.1840	.1847	1.487	104	9
52.50	53.00	.1956	.1991	1.442	113	10
58.00	58.30	.2350	.2373	1.316	203	11
	61.90		.2645		114	12
	62.60		.2679		210	13
63.80	63.80		.2792	1.207	211	14
	66.80		.3030		204	15
67.40	67.30	.3078	.3070	1.150	212	16
72.40	72.20	.3488	.3472	1.080	300	17
	73.00		.3338		213	18
73.50	73.90	.3580	.3572	1.066	301	19
76.20	76.70	.3807	.3830	1.034	302	20
	80.80		.4200		214	21
	82.20		.4321		303	22
85.70	85.40	.4625	.4643	0.938	220	23
89.50	89.80	.4999	.4982	0.906	304	24

$A = \frac{\lambda^2}{3a^2}$ where a = 3.76 A° and = 1.275 A°

Common factor for $\sin^2\theta$ values was 0.0383

Figure 22: Comparison of the experimental and refined profiles of hexagonal $SmD_{2.89}$

SMD 2.89 HEXAGONAL

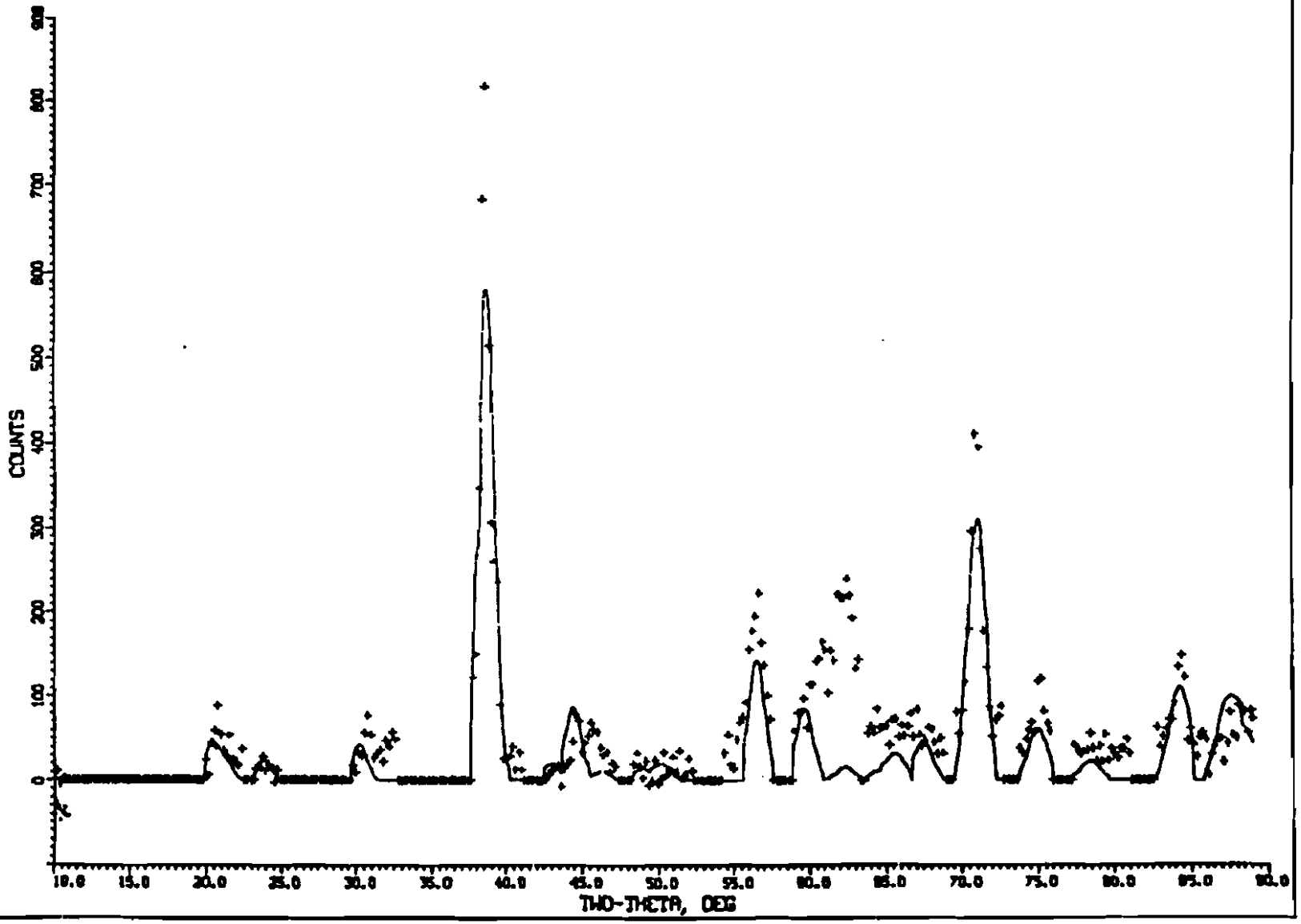

Figure 23: Comparison of the experimental and refined profiles of hexagonal $SmD_{2.99}$

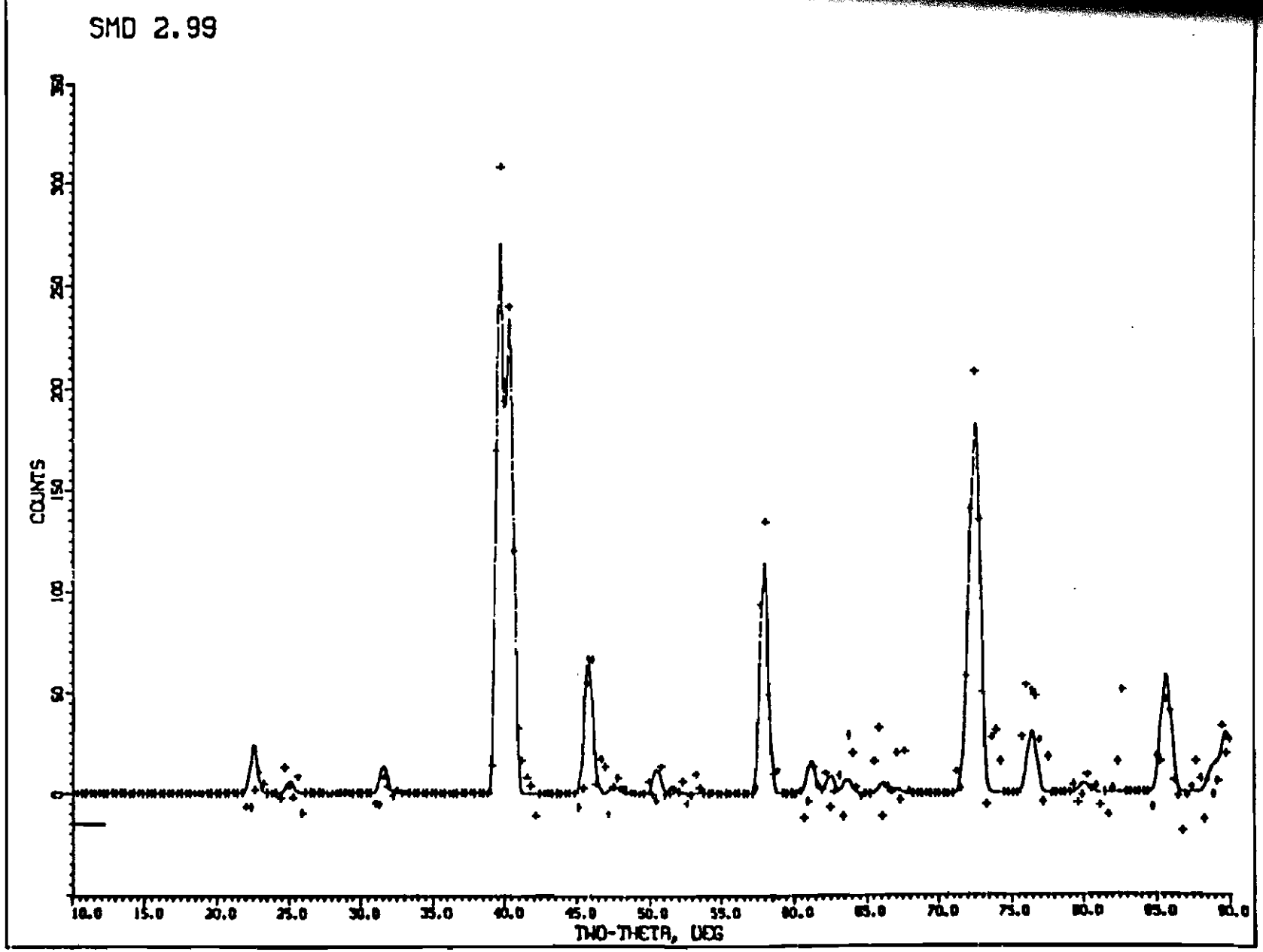
SMD 2.99
COUNTS
0
50
100
150
200
250
300
350
10.0
15.0
20.0
25.0
30.0
35.0
40.0
45.0
50.0
55.0
60.0
65.0
70.0
75.0
80.0
85.0
90.0
TWO-THETA, DEG

TABLE 8

ATOMIC POSITIONS IN THE HEXAGONAL SAMARIUM DEUTERIDES

Hexagonal		x	y	z	N	N_1
2.89	2 Sm	1/3	2/3	¼	0.06267 ± 0.01004	0.75207
	2 D	0	0	¼	0.06267 ± 0.01004	0.75207
	4 D	1/3	2/3	0.57714 ±0.00301	0.09884 ± 0.01004	0.59306
2.99	2 Sm	1/3	2/3	¼	0.09201 ± 0.00982	1.10412
	2 D	0	0	¼	0.09201 ± 0.00982	1.10412
	4 D	1/3	2/3	0.59630 ±0.00275	0.18871 ± 0.00982	1.13226

Figure 24: Comparison of the hexagonal intensities of $SmD_{2.89}$

H	K	L	POSN	INUC	IOBS	ESD
0	0	1	1048	0	266	142
0	0	2	2136	620	682	42
1	0	0	2228	145	443	36
1	0	1	2479	399	326	43
1	0	2	3120	535	648	48
0	0	3	3245	0	590	45
1	1	0	3936	4338	4800	68
1	0	3	3986	3262	3248	56
1	1	1	4092	0	241	32
0	0	4	4387	277	196	38
1	1	2	4534	1118	856	49
2	0	0	4582	15	50	4
2	0	1	4721	108	696	48
1	0	4	4987	254	189	38
2	0	2	5121	361	220	42
1	1	3	5205	0	189	33
0	0	5	5577	0	664	48
2	0	3	5742	1836	2974	72
1	1	4	6055	1179	2108	67
2	1	0	6212	2	603	32
2	1	1	6326	118	3873	79
2	0	4	6548	278	850	45
2	1	2	6661	753	1140	53
0	0	6	6837	723	1230	62
3	0	0	7167	2168	2265	47
2	1	3	7201	2760	2630	53
3	0	1	7274	0	503	34
3	0	2	7589	783	1741	64
2	1	4	7933	698	796	56
3	0	3	8105	0	695	48
2	2	0	8516	2066	2219	70
2	2	1	8617	0	442	36
3	0	4	8818	1126	928	49
2	2	2	8921	843	982	43
3	1	0	8956	31	42	2
3	1	1	9057	55	104	7

Figure 25: Comparison of the hexagonal intensities of $SmD_{2.99}$

H	K	L	POSN	INUC	IOBS	ESD
1	0	0	2255	142	12	26
1	0	1	2509	33	6	27
1	0	2	3159	33	42	26
1	1	0	3967	1663	1803	46
1	0	3	4036	1447	1535	44
1	1	1	4125	0	67	22
1	1	2	4575	433	309	29
2	0	0	4615	43	99	16
2	0	1	4757	22	35	30
1	0	4	5050	78	39	27
2	0	2	5163	22	0	0
1	1	3	5256	0	26	24
2	0	3	5794	786	893	47
1	1	4	6119	110	34	36
2	1	0	6251	59	27	33
2	1	1	6367	47	191	42
2	0	4	6612	36	128	39
2	1	2	6707	16	121	40
3	0	0	7210	612	650	35
2	1	3	7257	1147	1263	47
3	0	1	7318	0	161	26
3	0	2	7639	237	616	48
2	1	4	8001	37	0	0
3	0	3	3165	0	226	39
2	2	0	8564	498	354	48
2	2	1	8668	0	56	31
3	0	4	8890	103	0	0
2	2	2	8977	221	204	31
3	1	0	9007	49	42	8

TABLE 9

RELIABILITY FACTORS

H/M	R profile	R weighted	R expected
1.97	16.74	13.17	8.99
2.38	37.89	25.98	9.18
2.89cub	47.58	32.84	12.44
2.89hex	51.43	40.74	10.67
2.99	41.72	28.17	19.33

SECTION 6

DISCUSSION

$SmD_{1.97}$ and $SmD_{2.38}$ are both face centered cubic and belong to the proposed space group F 4/m 3 2/m. The site occupation factors for the $SmD_{1.97}$ sample shown in Table 5 indicate the deuterium to be located in the tetrahedral positions. Any additional deuterium goes into the octahedral positions as shown by the site occupation factor for the $SmD_{2.38}$ sample. $SmD_{1.97}$ shows good agreement between the experimental and calculated profile as indicated by the R factors in Table 9.

The agreement between the experimental and refined profiles represented by the R values in Table 9 for the $SmD_{2.38}$ sample is not good. Greis[9] claims that at a H/M of 2.34 a phase change occurs. Any stoichiometric determination was an average over the entire sample. It is plausible that some of the additional phase is present. A further indication of this is the doublet peak shown in the $SmD_{2.38}$ raw profile in Figure 13.

The lattice parameters for the deuterides should be smaller[9] than the a = 5.34 A for the hydrides. They should also provide evidence for the contraction of the lattice. The values a = 5.3274 A and a = 5.2977 A for $SmD_{1.97}$ and $SmD_{2.38}$ respectively, are reasonable values and support the contraction.

The hexagonal space group determined disagrees with that of Mansmann and Wallace.[95] The R factors representing the agreement between

the experimental and calculated profiles for the hexagonal space group $P\,6_3/m\,m\,c$ of the $SmD_{2.99}$ sample are not the best, but no other refinement resulted in better agreement. It should also be noted from Figure 15 and Figure 22 that the two larger peaks at two theta values equal to 34.1 and 83.0 are not indexed. These probably represent two of the superlattice peaks that have been found to occur in some of the hexagonal forms. Since the CWLS program tries to account for all data in the calculation of the R factors, the R values will reflect this problem. There is good enough agreement to conclude this space group represents the structure. No superlattice analysis has been made at this time.

The literature lattice parameters for the hexagonal unit cell are for the hydride a = 3.76 A and c = 6.79 A.[96] The values determined in this work are a = 3.7493 A and c = 6.7212 A and are in reasonable agreement since the deuteride parameters are generally smaller than the hydride parameters.

Both the cubic and hexagonal analysis were applied to $SmD_{2.89}$. Both patterns can be detected but neither can be refined to an acceptable agreement. There are no provisions in the computer programs available to refine a set of data using two different space groups. It is proposed that if these programs are written, the $SmD_{2.89}$ pattern would be a combination of the cubic and hexagonal. Because the present programs will not differentiate between the peaks of the two space groups and tries to incorporate all data in each refinement, neither the lattice sizes or any other parameters are valid. The site occupation factors for this sample from Table 8 show the Sm at(0, 0, 0) in the cubic refinement to be lower than expected and the Sm in the hexagonal to be

slightly lower than the expected(0, ½, ½). This may be an indication that this sample is on the average more hexagonal than cubic. The site occupation factor of 0.009 instead of the expected 0.04 in the Sm(0, 0, 0)position i.e., the origin of the unit cell, would indicate that the samarium atoms have moved. The only plausible explanation is a change to a different structure, i.e. the hexagonal, where the origin is located in a different relative position.

SECTION 7

SUMMARY

The purpose of this work was to determine the cubic and hexagonal space groups of the samarium hydrides and the positions of the atoms in the unit cell. This has been accomplished, but not to the best extent possible. This work was performed only as a preliminary effort in a project which will continue until the entire system is characterized. Samples will continue to be made at H/M stoichiometric ratios between 1.90 and 3.00 by 0.05 increments. Each sample will be analyzed with the structures determined here. In addition, superstructures will be determined and a tetragonal analysis will be performed.

It appears that there is some change occurring in the range of $SmD_{2.34}$ to $SmD_{2.38}$. It is not known whether this was from cubic to hexagonal or tetragonal and should be further investigated.

A computer program should be developed to handle two separate structures and to determine the extent to which each structure is present.

REFERENCES

1. E. Snape and F. E. Lynch, "Metal Hydrides Make Hydrogen Accessible - I, II," Chem. Tech. 10, 578 and 768 (1980).

2. R. H. Wiswall, Jr. and J. J. Reilly, "Metal Hydrides for Energy Storage," Proc. of the 7th Intersociety Energy Conversion Engineering Conf., Sept. 25-29, San Diego, Calif. (1972).

3. Westlake and Satterthwaite and Weaver, Physics Today 31 32 (1978).

4. Holley, Mulford, Ellinger, Koehler, and Zachariesen, J. Phys. Chem. 59, 1226 (1955).

5. Pebler and Wallace, J. Phys. Chem. 66, 148 (1962).

6. Holley, Mulford, Ellinger, Koehler, and Zachariesen, J. Phys. Chem. 59, 1226 (1955).

7. Moshe H. Mintz, "Thermodynamics and Statistical Mechanics of Some Hydrides of the Lanthanides and Actinides," NRCN-398 Israel Atomic Energy Commission, Beesheba.

8. Mannsmann and Wallace, J. Phys. 25, 454 (1964).

9. Pebler and Wallace, J. Phys. Chem. 66, 148 (1962).

10. Holley, Mulford, Ellinger, Koehler, and Zachariesen, J. Phys. Chem. 59, 1226 (1955).

11. Holley and Mulford, Ibid.

12. Holley and Mulford, Ibid.

13. Holley and Mulford, Ibid.

14. Pebler and Wallace, J. Phys. Chem. 66, 148 (1962).

15. Pebler and Wallace, Ibid.

16. Pebler and Wallace, Ibid.

17. Pebler and Wallace, Ibid.

18. C. E. Messer and M. K. Park, J. Less-Common Metals, 26, 235 (1972).

19. Mintz, Hierschler, and Hadari, J. Less-Common Metals, 48, 241 (1976).

20. Messer and Park, J. Less-Common Metals, 26, 235 (1972).

21. Mintz, Hadari, and Bixon, J. Less-Common Metals, 37, 331 (1974).

22. Mintz, Hierschler and Hadari, J. Less-Nommon Metals, 48, 241 (1976).

23. Korst and Warf, Inorg. Chem. 5, 1719 (1966).

24. Messer and Park, J. Less-Common Metals, 26, 235 (1972).

25. Moshe H. Mintz, "Thermodynamics and Statistical Mechanics of Some Hydrides of the Lanthanides and Actinides," NRCN-398 Israel Atomic Energy Commission, Beesheba.

26. O. Greis, P. Knappe, and H. Muller, (to be published).

27. O. Greis, P. Knappe, and H. Muller, (to be published).

28. Kubota and Wallace, J. Appl. Phys. 34, 1348 (1963).

29. Holley and Mulford, J. Phys. Chem. 59, 1226 (1955).

30. Holley and Mulford, Ibid.

31. Pebler and Wallace, J. Phys. Chem. 66, 148 (1962).

32. Korst and Warf, Inorg. Chem. 5, 1719 (1966).

33. Messer and Park, J. Less-Common Metals, 26, 235 (1972).

34. Mintz, Hierschler and Hadari, J. Less-Common Metals, 48, 241 (1976).

35. C. L. Huffine, "Fabrication of Hydrides," in Metal Hydrides, Mueller, Blackledge, and Libowitz, Academic Press, N.Y., (1968), pp. 675-744.

36. International Tables for X-Ray Crystallography, Vol 1: Symmetry Groups, Kynoch Press, Birmingham, England, (1965).

37. Nuclides and Isotopes, General Electric, (1977), pp. 11.

38. G. E. Bacon, Neutron Diffraction, Clarendon Press, Oxford, (1975), pp. 3.

39. Mandelcorn, Nonstoichiometric Compounds, Academic Press, N.Y., (1964), pp. 41.

40. H. Lipson and H. Steeple, Interpretation of X-Ray Powder Diffraction Patterns, Macmillian, N.Y., (1970), pp. 111.

41. G. M. Barrow, Physical Chemistry, "Diffraction Methods," McGraw-Hill, N.Y., (1974), pp. 529.

42. Blackledge, Metal Hydrides, Academic Press, N.Y., (1968), pp. 7-8.

43. Mandelcorn, Nonstoichiometric Compounds, Academic Press, N.Y., (1964), pp. 42.

44. Bacon, Neutron Diffraction, Clarendon Press, Oxford, (1975), pp. 38-41.

45. B. D. Cullity, Elements of X-Ray Diffraction, 2nd Edition, Addison-Wesley Pub. Co., Reading, Mass., (1978), pp. 139.

46. Cullity, Ibid., pp. 115-126.

47. Lipson and Steeple, Interpretation of X-Ray Powder Diffraction Patterns, Macmillan, N.Y., (1970), pp. 214-217.

48. Lipson and Steeple, Ibid., pp. 203-210.

49. B. D. Cullity, Elements of X-Ray Diffraction, 2nd Edition, Addison-Wesley Pub. Co., Reading, Mass., (1978), pp. 127.

50. L. I. Mirkin Handbook of X-Ray Analysis of Polycrystalline Materials, Consultants Bureau, N.Y., (1964), pp. 380.

51. International Tables for X-Ray Crystallography, Vol 1: Symmetry Group, Kynoch Press, Birmingham, England, (1965).

52. Lipson and Steeple, Interpretation of X-Ray Powder Diffraction Patterns, Macmillan, N.Y., (1970), pp. 322-323.

53. B. D. Cullity, Elements of X-Ray Diffraction, 2nd Edition, Addison-Wesley Pub. Co., Reading, Mass., (1978), pp. 523.

54. Bacon, Neutron Diffraction, Clarendon Press, Oxford, (1975), pp. 71.

55. Mandelcorn, Nonstoichiometric Compounds, Academic Press, N.Y., (1964), pp. 43.

56. B. D. Cullity, Elements of X-Ray Diffraction, 2nd Edition, Addison-Wesley Pub. Co., Reading, Mass., (1978), pp. 135-139.

57. G. H. Stout and L. H. Jensen, X-Ray Structure Determination, Macmillan Co., N.Y., (1968), pp. 205-208 and 449-450.

58. M. J. Buerger, Crystal Structure Analysis, Wiley, N.Y., (1960), pp. 231-237.

59. B. D. Cullity, Elements of X-Ray Diffraction, 2nd Edition, Addison-Wesley Pub. Co., Reading, Mass., (1978), pp. 127.

60. G. H. Stout and L. H. Jensen, X-Ray Structure Determination, Macmillan Co., N.Y., (1968), pp. 195-199.

61. Lipson and Steeple, Interpretation of X-Ray Powder Diffraction Patterns, Macmillan, N.Y., (1970), pp. 199-200.

62. G. H. Stout and L. H. Jensen, X-Ray Structure Determination, Macmillan Co., N.Y., (1968), pp. 207-208.

63. Stout and Jensen, Ibid., pp. 204-208.

64. B. D. Cullity, Elements of X-Ray Diffraction, 2nd Edition, Addison-Wesley Pub. Co., Reading, Mass., (1978), pp. 324-340.

65. Mirkin, Handbook of X-Ray Analysis of Polycrystalline Materials, Consultants Bureau, N.Y., (1964), pp. 90-311.

66. Lipson and Steeple, Interpretation of X-Ray Powder Diffraction Patterns, Macmillan, N.Y., (1970), pp. 312-315.

67. Mirkin, Handbook of X-Ray Analysis of Polycrystalline Materials, Consultants Bureau, N.Y., (1964), pp. 207-224, 237-238, 254-257, and 272-274.

68. Lipson and Steeple, Interpretation of X-Ray Powder Diffraction Patterns, Macmillan, N.Y., (1970), pp. 113-156.

69. Mirkin, Handbook of X-Ray Analysis of Polycrystalline Materials, Consultants Bureau N.Y., (1964).

70. B. D. Cullity, Elements of X-Ray Diffraction, 2nd Edition, Addison-Wesley Pub. Co., Reading, Mass., (1978), pp. 324-340.

71. Cullity, Ibid., pp. 330-332.

72. Lipson and Steeple, Interpretation of X-Ray Powder Diffraction Patterns, MacMillan, N.Y., (1970), pp. 148-149.

73. G. W. Bunn, Chemical crystallography, London, (1945).

74. M. V. Schwarz and O. Summa, Praktische Auswertungshilfsmittel fur Feinstrukturun-tersuuchungen, Muchen, (1932).

75. Lipson and Steeple, Interpretation of X-Ray Powder Diffraction Patterns, MacMillan, N.Y., (1970), pp. 149-151.

76. Lipson and Steeple, Ibid., pp. 144-148.

77. Mirkin, Handbook of X-Ray Analysis of Polycrystalline Materials, Consultants Bureau, N.Y., (1964), pp. 224-233, 242-248, 258-267, 278-283, 287-295 and 296-297.

78. B. D. Cullity, Elements of X-Ray Diffraction, 2nd Edition, Addison-Wesley Pub. Col, Reading, Mass., (1978), pp. 342-343.

79. Cullity, Ibid., pp. 343-345.

80. Mirkin, Handbook of X-Ray Analysis of Polycrystalline Materials, Consultants Bureau, N.Y., (1964), pp. 207, 235-236, and 249-253.

81. Mirkin, Ibid., pp. 406-424.

82. Mirkin, Ibid., pp. 348-370.

83. International Tables for X-Ray Crystallography, Vol 1: Symmetry Groups, Kynoch Press, Birmingham, England, (1965).

84. Lipson and Steeple, Interpretation of X-Ray Powder Diffraction Patterns, MacMillan, N.Y., (1970), pp. 236-240.

85. G. H. Stout and L. H. Jensen, X-Ray Structure Determination, MacMillan Co., N.Y., (1968), pp. 385-394.

86. B. D. Cullity, Elements of X-Ray Diffraction, 2nd Edition, Addison-Wesley Pub. Co., Reading, Mass., (1978), pp. 360-363.

87. H. M. Rietveld, J. Appl Cryst 2, 65 (1969).

88. Lipson and Steeple, Interpretation of X-Ray Powder Diffraction Patterns, MacMillan, N.Y., (1970), pp. 236.

89. G. E. Bacon, Neutron Diffraction, Clarendon Press, Oxford, (1975), pp. 13.

90. Bacon, Ibid., pp. 14.

91. Mirkin, Handbook of X-Ray Analysis of Polycrystalline Materials, Consultants Bureau, N.Y., (1964), pp. 264.

92. Mirkin, Ibid.

93. O. Greis, P. Knappe, and H. Muller, (to be published).

94. G. G. Libowitz, The Solid State Chemistry of Binary Metal Hydrides, W. A. Benjamen, Inc., N.Y., (1965).

95. Mannsmann and Wallace, J. Phys. 25, 454 (1964).

96. O. Greis, P. Knappe, and H. Muller, (to be published).

APPENDIX A

N Values For Various Crystal Systems

Cubic $N = h^2 + k^2 + l^2$ P	Cubic F	Cubic I	Tetragonal $N = h^2 + k^2$	Hexagonal $N = h^2 + hk + k^2$
hkl	*hkl*	*hkl*	*hk*	*hk*
100			10	10
110		110	11	
111	111			11
200	200	200	20	20
210			21	
211		211		
				21
220	220	220	22	
300			30	30
221				
310		310	31	
311	311			
222	222	222		22
320			32	31
321		321		
400	400	400	40	40
410			41	
322				
411		411		
330		330	33	
331	331			32
420	420	420	42	
421				41
332		332		
422	422	422		
500			50	50
430			43	
510		510	51	
431		431		
511	511			33
333	333			
				42
520			52	
432				
521		521		
				51
440	440	440		
522			44	
441				

N	Cubic $N = h^2 + k^2 + l^2$ P	Cubic F	Cubic I	Tetragonal $N = h^2 + k^2$	Hexagonal $N = h^2 + hk$
	hkl	*hkl*	*hkl*	*hk*	*hk*
34	530		530	53	
34	433		433		
35	531	531			
36	600	600	600	60	60
36	442	442	442		
37	610			61	43
38	611		611		
38	532		532		
39					52
40	620	620	620	62	
41	621				
41	540			54	
41	443				
42	541		541		
43	533	533			61
44	622	622	622		
45	630			63	
45	542				
46	631		631		
47					
48	444	444	444		44
49	700			70	70
49	632				53
50	710		710	71	
50	550		550	55	
50	543		543		
51	711	711			
51	551	551			
52	640	640	640	64	62
53	720			72	
53	641				
54	721		721		
54	633		633		
54	552		552		
55					
56	642	642	642		
57	722				71
57	644				
58	730		730	73	
59	731	731			
59	553	553			

Cubic $N = h^2 + k^2 + l^2$ P hkl	Cubic F hkl	Cubic I hkl	Tetragonal $N = h^2 + k^2$ hk	Hexagonal $N = h^2 + hk + k^2$ hk
650			65	54
643				
732		732		
651		651		
				63
800	800	800	80	80
810			81	
740			74	
652				
811		811		
741		741		
554		554		
733	733			72
820	820	820	82	
644	644	644		
821				
742				
653		653		
822	822	822		
660	660	660	66	
830			83	81
661				
831		831		
750		750	75	
743		743		
751	751			55
555	555			
662	662	662		64
832				
654				
752		752		
				73
840	340	840	84	
900			90	90
841				
744				
663				

N	Cubic $N = h^2 + k^2 + l^2$ P hkl	Cubic F hkl	Cubic I hkl	Tetragonal $N = h^2 + k^2$ hk	Hexago $N = h^2 + hk$ hk
82	910		910	91	
82	833		833		
83	911	911			
83	753	753			
84	842	842	842		82
85	920			92	
85	760			76	
86	921		921		
86	761		761		
86	655		655		
87					
88	664	664	664		
89	922			85	
89	850				
89	843				
89	762				
90	930		930	93	
90	851		851		
90	754		754		
91	931	931			65
91					91
92					
93	852				74
94	932		932		
94	763		763		
95					
96	844	844	844		
97	940			94	83
97	665				
98	941		941		
98	853		853		
98	770		770	77	
99	933	933			
99	771	771			
99	755	755			
100	10,00	10,00	10,00	10,0	10,0
100	860	860	860	86	

APPENDIX B

The Computer Programs: CWPREF, CWLS, and CWPLOT

CWPREF

The CWPREF program handles the raw data, indexing each reflection and drawing the raw profile.

Input Parameters: Wavelength

Unit Cell Parameters

Background Profile

Miller indices of the reflections

Multiplicities of indices

Gaussian peak parameters: U, V, W

Two Theta Values and their corresponding neutron count, i.e. raw data

After subtracting off the background, the counts at each position are weighted by the factor $1/\sigma_i^2$ where σ is the estimated standard deviation. The program then determines the halfwidth parameters and the shape of the peaks. Then it determines which reflections contribute to each peak and its corresponding two theta values. The experimental profile is then stored on a tape for use in the CWLS and CWPLOT programs.

CWLS

The CWLS program calculates a profile by least squares methods and then compares this profile with the experimental profile.

Input Parameters: Wavelength

Centrosymmetry

General equivalent positions of the space group in matrix form

Translation Vectors in matrix form

Neutron scattering factors

x, y, z values for the general positions

Cell parameters

U, V, W

Site occupation factor*

Scale factor

Overall and individual temperature factors

Zeropoint

Codewords used to indicate the parameters to be refined and the order of refinement.

CWLS calculates the observed and calculated structure factors and then rescales them in the next cycles by use of the linear rescale factor

$$LRS = \Sigma |F_c| / \Sigma |F_o|$$

First, initial values are chosen and inserted in the data program (CWINS2). By using a series of codewords, the analyst will have the program adjust in successive steps, any of the parameters designated by the codeword. After each series of refinements, the

---

*Site occupation factors represent the number of atoms to be found at each location. It is usually determined by dividing the number of atoms in each position by the total number of symmetry operators.

new values are then placed into the input file and used in the next series of refinements. After each cycle the R values are determined and their effect on the refinement noted.

The order of parameters can be varied. The usual order succeeds as 1) scale factor, 2) zeropoint, 3) cell sizes, 4) overall temperature factor, 5) atomic positions, 6) U, V, W, site occupation factors, individual temperature factors, etc.

CWPLOT

The CWPLOT program plots the raw data and the calculated profile on the same axis. Unfortunately, it plots only the portions of the profile it is comparing, not the entire profile. It does not, therefore, account for all the peaks in the raw profile nor allow for missing peaks. CWPLOT also draws a difference profile that is not included on the graphs presented in this thesis because it reduces the clarity of the graph.

APPENDIX C

The Method of Least Squares

METHOD OF LEAST SQUARES

The method of least squares is a method that determines the best values of the parameters by minimizing the sums of the squares of the weighted differences between the observed and calculated values of all the points.

In diffraction, the quantity to be minimized is

$$D = \sum_{hkl} W_{hkl} \left(|F_o| - |k\ F_c|\right)^2 \qquad (1)$$

where W_{hkl} is the weight of the observation and $\sum_{hkl}$ is the summation over all points for the observed reflections.

Minimization is achieved by taking the derivative with respect to each parameter and equating it to zero. This leads to the n number of normal equations:

$$\sum_{hkl} W_{hkl} \left(|F_o| - |k\ F_c(p_1\ p_2 \ldots p_n)|\right) \frac{\partial |kF_c(p_1 \ldots p_n)|}{\partial p_j} = 0 \qquad (2)$$

for j = 1,2..n.

The function $|F_c|$ is expressed as a Taylor series and neglects second and higher orders so that

$$|k\ F_c(p_1 \ldots p_n)| = |k\ F_c(a_1 \ldots a_n)| + \frac{\partial |kF_c|}{\partial p_1} \Delta p_1 + \ldots \qquad (3)$$

$$+ \frac{\partial |kF_c|}{\partial p_n} \Delta p_n$$

where $p_1 \ldots p_n$ is any scale, position, thermal parameters, etc. and $\Delta p_j = p_j - a_j$. Substituting equation 3 into equation 2 and expanding and rearranging produces a series of equations called the normal equations. These equations can be solved simultaneously for the most probable values of the parameters. The normal equations can be written in matrix form as

$$\begin{aligned} a_{11} x_1 + a_{12} x_2 + \ldots + a_{1n} x_n &= u_1 \\ a_{21} x_1 + a_{22} x_2 + \ldots + a_{2n} x_n &= u_2 \\ \vdots \qquad\qquad \vdots \qquad\qquad & \\ a_{n1} x_1 + a_{n2} x_2 + \ldots + a_{nn} x_n &= u_n \end{aligned} \tag{4}$$

where $a_{ij} = \sum_{r=1}^{m} Wr \frac{\partial |F_{cr}|}{\partial p_i} \frac{\partial |F_{cr}|}{\partial p_j}$

$x_j = \Delta p_j$

$u_i = \sum_{r=1}^{m} Wr \, (\Delta F_r) \frac{\partial (F_{cr})}{\partial p_i}$

If these equations have a solution, then there exists an inverse matrix such that multiplication of the two matrices = 1. Then the diagonal of the inverse, $b_{ii} = 1/a_{ii}$, can be shown to be a measure of the correlation of the parameters i and j. The correlation coefficient is defined as

$$\delta_{ij} = b_{ij} / (b_{ii})^{\frac{1}{2}} (b_{jj})^{\frac{1}{2}}$$

The correlation matrix is used by the CWLS program to determine the solution to the normal equations and thus determine the best value for the parameters refined.

APPENDIX D

Estimated Standard Deviations

ESTIMATED STANDARD DEVIATIONS

The equation for calculating the standard deviation, σ, for any parameter, p, is

$$\sigma_{pi} = \left[b_{ii} \left(\sum_{r=1}^{m} Wr \ \Delta Fr^2 \right) / (m-n) \right]^{\frac{1}{2}}$$

where b is the ith diagonal element of the inverse matrix (See Appendix C),

Wr is the weight of the rth ΔF,

m is the number of observations,

n is the number of parameters,

and $w = 1/\sigma_{fo}^{2}$.

During the least squares refinements, the estimated standard deviations are also calculated for each parameter refined.

APPENDIX E

Samarium Metal Analysis

ANALYSIS OF SM 154 ISOTOPE

Isotopic Analysis

Isotope	Percent	Precision
144	0.02	± 0.01
147	0.14	± 0.02
148	0.12	± 0.02
149	0.17	± 0.02
150	0.12	± 0.02
152	0.74	± 0.05
154	98.69	± 0.10

Rare Earth Analysis

Element	Percent	Element	Percent
Yb	0.002	Gd	<0.02
Y	<0.005	Tb	<0.05
La	<0.02	Dy	<0.1
Ce	<0.2	Ho	<0.02
Pr	<0.05	Er	<0.005
Nd	<0.05	Tm	<0.03
Eu	<0.005	Lu	<0.005

Spectrographic Analysis

Element	Percent	Element	Percent
Ca	0.01	Mn	< 0.02
Ag	< 0.01	Mo	< 0.02
Al	< 0.05	Na	< 0.01
B	< 0.01	Ni	<0.05
Ba	<0.01	Pb	<0.02
Be	<0.001	Pt	<0.05
Bi	<0.02	Rb	<0.02
Cb	<0.05	Sb	<0.05
Co	<0.05	Si	<0.01
Cr	<0.05	Sn	<0.02
Cs	<0.05	Sr	<0.01
Cu	<0.01	Ta	<0.05
Fe	<0.02	Ti	<0.01
Ge	<0.05	V	<0.02
Hg	<0.05	W	<0.05
K	<0.01	Zn	<0.2
Mg	<0.01	Zr	<0.05
Li	<0.005		

APPENDIX F

Raw Diffraction Data: Two Theta versus Neutron Counts

Raw Neutron Diffraction Data for $SmD_{1.97}$ at λ =1.275

2000	85	2460	73	2920	68
2010	82	2470	73	2930	73
2020	114	2480	86	2940	76
2030	108	2490	62	2950	72
2040	76	2500	58	2960	82
2050	70	2510	67	2970	54
2060	66	2520	82	2980	75
2070	57	2530	93	2990	67
2080	49	2540	73	3000	63
2090	52	2550	68	3010	64
2100	70	2560	86	3020	65
2110	66	2570	83	3030	53
2120	65	2580	65	3040	65
2130	58	2590	78	3050	58
2140	67	2600	85	3060	99
2150	61	2610	82	3070	71
2160	56	2620	70	3080	77
2170	46	2630	74	3090	73
2180	123	2640	74	3100	68
2190	106	2650	78	3110	76
2200	85	2660	58	3120	85
2210	92	2670	77	3130	75
2220	81	2680	79	3140	84
2230	81	2690	48	3150	69
2240	76	2700	63	3160	80
2250	80	2710	78	3170	75
2260	67	2720	75	3180	88
2270	86	2730	81	3190	102
2280	86	2740	106	3200	87
2290	92	2750	87	3210	85
2300	85	2760	104	3220	78
2310	67	2770	77	3230	93
2320	91	2780	71	3240	83
2330	78	2790	68	3250	68
2340	113	2800	73	3260	85
2350	157	2810	67	3270	99
2360	292	2820	72	3280	89
2370	382	2830	59	3290	104
2380	324	2840	54	3300	78
2390	299	2850	67	3310	94
2400	187	2860	68	3320	98
2410	127	2870	74	3330	114
2420	111	2880	83	3340	97
2430	90	2890	61	3350	91
2440	91	2900	63	3360	100
2450	69	2910	81	3370	107

3380	125	3840	99	4300	85
3390	110	3850	116	4310	90
3400	110	3860	83	4320	101
3410	107	3870	110	4330	88
3420	95	3880	98	4340	111
3430	100	3890	95	4350	96
3440	97	3900	125	4360	95
3450	123	3910	264	4370	83
3460	102	3920	556	4380	113
3470	109	3930	949	4390	105
3480	103	3940	1139	4400	102
3490	112	3950	969	4410	91
3500	100	3960	759	4420	99
3510	104	3970	484	4430	93
3520	113	3980	297	4440	93
3530	98	3990	190	4450	100
3540	109	4000	142	4460	96
3550	99	4010	146	4470	97
3560	116	4020	137	4480	109
3570	94	4030	127	4490	109
3580	93	4040	124	4500	91
3590	93	4050	94	4510	81
3600	125	4060	94	4520	82
3610	112	4070	80	4530	91
3620	96	4080	82	4540	106
3630	92	4090	88	4550	105
3640	110	4100	90	4560	103
3650	107	4110	98	4570	107
3660	88	4120	95	4580	105
3670	101	4130	119	4590	99
3680	108	4140	112	4600	98
3690	117	4150	93	4610	83
3700	100	4160	96	4620	102
3710	120	4170	104	4630	157
3720	80	4180	109	4640	205
3730	102	4190	110	4650	307
3740	92	4200	121	4660	298
3750	79	4210	94	4670	329
3760	102	4220	95	4680	280
3770	78	4230	97	4690	227
3780	98	4240	83	4700	139
3790	96	4250	90	4710	100
3800	112	4260	77	4720	79
3810	96	4270	99	4730	99
3820	83	4280	73	4740	105
3830	96	4290	94	4750	103

4760	102	5220	98	5680	210
4770	101	5230	117	5690	279
4780	113	5240	117	5700	317
4790	105	5250	102	5710	317
4800	80	5260	101	5720	309
4810	85	5270	100	5730	216
4820	79	5280	87	5740	191
4830	101	5290	98	5750	135
4840	100	5300	97	5760	137
4850	84	5310	108	5770	129
4860	99	5320	112	5780	112
4870	108	5330	12	5790	109
4880	106	5340	109	5800	115
4890	97	5350	115	5810	128
4900	117	5260	116	5820	126
4910	97	5370	100	5830	133
4920	117	5380	113	5840	109
4930	102	5390	101	5850	159
4940	98	5400	85	5860	121
4950	78	5410	107	5870	106
4960	96	5420	94	5880	124
4970	99	5430	104	5890	132
4980	91	5440	106	5900	117
4990	99	5450	109	5910	126
5000	90	5460	104	5920	120
5010	97	5470	94	5930	140
5020	92	5480	119	5940	136
5030	100	5490	105	5950	138
5040	111	5500	98	5960	125
5050	78	5510	130	5970	129
5060	85	5520	99	5980	127
5070	85	5530	96	5990	122
5080	93	5540	103	6000	131
5090	111	5550	100	6010	116
5100	100	5560	108	6020	131
5110	89	5570	110	6030	126
5120	126	5580	91	6040	141
5130	95	5590	117	6050	130
5140	112	5600	102	6060	135
5150	113	5610	91	6070	126
5160	81	5620	111	6080	127
5170	100	5630	110	6090	129
5180	91	5640	105	6100	134
5190	95	5650	126	6110	136
5200	98	5660	116	6120	120
5210	95	5670	140	6130	129

6140	128	6600	162	7060	142
6150	136	6610	183	7070	134
6160	142	6620	168	7080	119
6170	124	6630	163	7090	129
6180	135	6640	156	7100	129
6190	150	6650	161	7110	148
6200	142	6660	172	7120	197
6210	148	6670	158	7130	251
6220	176	6680	167	7140	381
6230	133	6690	184	7150	534
6240	179	6700	161	7160	606
6250	216	6710	167	7170	615
6260	257	6720	167	7180	611
6270	295	6730	146	7190	466
6280	279	6740	165	7200	321
6290	261	6750	171	7210	241
6300	216	6760	171	7220	199
6310	192	6770	153	7230	128
6320	167	6780	165	7240	129
6330	175	6790	157	7250	122
6340	145	6800	150	7260	146
6350	161	6810	140	7270	121
6360	172	6820	157	7280	136
6370	160	6830	134	7290	133
6380	174	6840	163	7300	140
6390	173	6850	174	7310	113
6400	151	6860	134	7320	125
6410	152	6870	156	7330	129
6420	150	6880	161	7340	159
6430	179	6890	159	7350	112
6440	179	6900	147	7360	125
6450	180	6910	147	7370	114
6460	203	6920	132	7380	118
6470	187	6930	160	7390	108
6480	192	6940	160	7400	115
6490	195	6950	140	7410	121
6500	180	6960	144	7420	98
6510	166	6970	141	7430	116
6520	170	6980	142	7440	99
6530	160	6990	145	7450	118
6540	172	7000	142	7460	122
6550	192	7010	138	7470	129
6560	189	7020	139	7480	132
6570	179	7030	141	7490	125
6580	160	7040	133	7500	126
6590	183	7050	122	7510	104

7520	108	7980	87	8440	118
7530	127	7990	111	8450	128
7540	122	8000	101	8460	124
7550	100	8010	85	8470	172
7560	114	8020	101	8480	194
7570	121	8030	110	8490	287
7580	118	8040	120	8500	308
7590	142	8050	115	8510	297
7600	127	8060	112	8520	278
7610	153	8070	96	8530	246
7620	142	8080	99	8540	199
7630	147	8090	114	8550	176
7640	159	8100	124	8560	160
7650	188	8110	116	8570	132
7660	208	8120	114	8580	113
7670	228	8130	105	8590	129
7680	254	8140	98	8600	108
7690	210	8150	112	8610	119
7700	206	8160	104	8620	111
7710	170	8170	110	8630	109
7720	142	8180	98	8640	124
7730	103	8190	117	8650	117
7740	104	8200	99	8660	128
7750	114	8210	105	8670	129
7760	105	8220	100	8680	115
7770	132	8230	111	8690	143
7780	107	8240	114	8700	114
7790	110	8250	105	8710	111
7800	132	8260	87	8720	122
7810	114	8270	94	8730	111
7820	123	8280	74	8740	117
7830	113	8290	115	8750	108
7840	92	8300	127	8760	115
7850	105	8310	99	8770	122
7860	117	8320	101	8780	120
7870	113	8330	107	8790	129
7880	107	8340	130	8800	105
7890	103	8350	110	8810	104
7900	113	8360	117	8820	140
7910	123	8370	104	8830	125
7920	109	8380	92	8840	108
7930	116	8390	112	8850	122
7940	133	8400	98	8860	115
7950	112	8410	121	8870	109
7960	100	8420	103	8880	114
7970	117	8430	104	8890	106

8900	120
8910	114
8920	102
8930	114
8940	93
8950	134
8960	149
8970	157
8980	193
8990	217
9000	249

Raw Diffraction Data for $SmD_{2.38}$ at λ =1.275

1000	285	1480	235	1960	333
1010	153	1490	254	1970	357
1020	183	1500	253	1980	320
1030	170	1510	271	1990	297
1040	193	1520	296	2000	307
1050	174	1530	269	2010	282
1060	198	1540	265	2020	275
1070	157	1550	288	2030	253
1080	184	1560	311	2040	322
1090	178	1570	339	2050	265
1100	150	1580	334	2060	274
1110	163	1590	302	2070	280
1120	162	1600	328	2080	288
1130	167	1610	354	2090	242
1140	159	1620	310	2100	275
1150	169	1630	352	2110	252
1160	196	1640	298	2120	259
1170	197	1650	323	2130	216
1180	193	1660	344	2140	263
1190	170	1670	319	2150	296
1200	197	1680	335	2160	337
1210	195	1690	366	2170	315
1220	187	1700	354	2180	339
1230	173	1710	342	2190	299
1240	182	1720	342	2200	264
1250	197	1730	351	2210	224
1260	156	1740	355	2220	242
1270	180	1750	351	2230	269
1280	201	1760	343	2240	276
1290	196	1770	337	2250	306
1300	213	1780	351	2260	272
1310	175	1790	366	2270	263
1320	196	1800	352	2280	215
1330	235	1810	338	2290	219
1340	228	1820	348	2300	277
1350	215	1830	332	2310	201
1360	219	1840	317	2320	202
1370	209	1850	355	2330	227
1380	221	1860	365	2340	191
1390	234	1870	350	2350	200
1400	235	1880	342	2360	200
1410	230	1890	342	2370	210
1420	231	1900	345	2380	205
1430	223	1910	323	2390	194
1440	234	1920	366	2400	192
1450	204	1930	341	2410	171
1460	228	1940	365	2420	183
1470	257	1950	335	2430	195

2440	178	2910	134	3380	313
2450	179	2920	161	3390	308
2460	169	2930	148	3400	330
2470	155	2940	158	3410	351
2480	184	2950	143	3420	394
2490	175	2960	144	3430	358
2500	228	2970	117	3440	354
2510	176	2980	162	3450	344
2520	195	2990	156	3460	357
2530	187	3000	135	3470	312
2540	185	3010	158	3480	292
2550	182	3020	147	3490	285
2560	170	3030	160	3500	335
2570	166	3040	145	3510	321
2580	164	3050	172	3520	338
2590	145	3060	149	3530	315
2600	171	3070	153	3540	316
2610	157	3080	181	3550	317
2620	176	3090	183	3560	293
2630	160	3100	153	3570	287
2640	150	3110	160	3580	290
2650	153	3120	164	3590	299
2660	140	3130	192	3600	301
2670	151	3140	201	3610	290
2680	169	3150	211	3620	285
2690	163	3160	211	3630	312
2700	160	3170	206	3640	301
2710	143	3180	233	3650	279
2720	166	3190	216	3660	303
2730	143	3200	234	3670	306
2740	170	3210	219	3680	306
2750	159	3220	267	3690	287
2760	174	3230	233	3700	242
2770	156	3240	238	3710	301
2780	158	3250	247	3720	286
2790	144	3260	260	3730	262
2800	150	3270	246	3740	260
2810	161	3280	285	3750	268
2820	129	3290	243	3760	261
2830	146	3300	262	3770	250
2840	128	3310	263	3780	260
2850	129	3320	264	3790	263
2860	143	3330	253	3800	247
2870	154	3340	292	3810	232
2880	151	3350	276	3820	273
2890	164	3360	286	3830	253
2900	147	3370	272	3840	255

3850	280	4320	217	4790	216
3860	276	4330	230	4800	217
3870	285	4340	228	4810	224
3880	249	4350	241	4820	234
3890	285	4360	222	4830	213
3900	314	4370	226	4840	241
3910	293	4380	234	4850	236
3920	326	4390	229	4860	219
3930	454	4400	237	4870	212
3940	726	4410	204	4880	226
3950	1009	4420	239	4890	227
3960	1167	4430	223	4900	233
3970	1104	4440	190	4910	233
3980	991	4450	217	4920	220
3990	797	4460	221	4930	217
4000	766	4470	215	4940	246
4010	738	4480	214	4950	243
4020	896	4490	224	4960	260
4030	1019	4500	199	4970	227
4040	946	4510	213	4980	255
4050	750	4520	226	4990	232
4060	593	4530	250	5000	227
4070	477	4540	285	5010	219
4080	338	4550	307	5020	255
4090	332	4560	357	5030	256
4100	334	4570	436	5040	241
4110	273	4580	348	5050	240
4120	249	4590	348	5060	221
4130	287	4600	331	5070	234
4140	274	4610	305	5080	228
4150	283	4620	271	5090	237
4160	281	4630	249	5100	233
4170	273	4640	267	5110	264
4180	231	4650	245	5120	229
4190	247	4660	218	5130	235
4200	233	4670	249	5140	260
4210	232	4680	258	5150	246
4220	205	4690	209	5160	255
4230	255	4700	231	5170	237
4240	211	4710	241	5180	237
4250	247	4720	268	5190	247
4260	233	4730	241	5200	257
4270	204	4740	224	5210	216
4280	230	4750	247	5220	226
4290	201	4760	198	5230	240
4300	216	4770	261	5240	267
4310	222	4780	239	5250	224

5260	241	5740	304	6220	353
5270	217	5750	354	6230	400
5280	258	5760	433	6240	366
5290	225	5770	490	6250	353
5300	230	5780	578	6260	390
5310	239	5790	608	6270	353
5320	226	5800	554	6280	380
5330	213	5810	534	6290	387
5340	244	5820	477	6300	379
5350	224	5830	388	6310	371
5360	228	5840	357	6320	348
5370	265	5850	365	6330	419
5380	257	5860	308	6340	412
5390	240	5870	321	6350	421
5400	252	5880	311	6360	457
5410	236	5890	288	6370	469
5420	263	5900	314	6380	462
5430	244	5910	299	6390	436
5440	253	5920	325	6400	457
5450	235	5930	339	6410	461
5460	256	5940	324	6420	435
5470	240	5950	349	6430	473
5480	228	5960	298	6440	450
5490	252	5970	301	6450	420
5500	223	5980	315	6460	428
5510	230	5990	279	6470	400
5520	243	6000	322	6480	412
5530	258	6010	317	6490	434
5540	237	6020	342	6500	429
5550	283	6030	313	6510	439
5560	280	6040	332	6520	435
5570	249	6050	338	6530	459
5580	276	6060	331	6540	415
5590	249	6070	354	6550	457
5600	295	6080	344	6560	445
5610	249	6090	319	6570	461
5620	239	6100	319	6580	432
5630	269	6110	331	6590	458
5640	235	6120	339	6600	432
5650	282	6130	374	6610	405
5660	273	6140	372	6620	413
5670	279	6150	355	6630	413
5680	282	6160	359	6640	409
5690	269	6170	349	6650	437
5700	265	6180	373	6660	430
5710	267	6190	395	6670	430
5720	285	6200	384	6680	441
5730	315	6210	365	6690	402

6700	429	7170	385	7640	313
6710	409	7180	445	7650	266
6720	447	7190	511	7660	277
6730	434	7200	547	7670	326
6740	382	7210	543	7680	275
6750	435	7220	599	7690	267
6760	432	7230	655	7700	245
6770	414	7240	579	7710	263
6780	384	7250	731	7720	240
6790	402	7260	741	7730	252
6800	436	7270	649	7740	260
6810	371	7280	580	7750	247
6820	405	7290	497	7760	239
6830	398	7300	412	7770	251
6840	387	7310	382	7780	235
6850	373	7320	345	7790	256
6860	424	7330	340	7800	259
6870	373	7340	314	7810	242
6880	375	7350	336	7820	237
6890	340	7360	332	7830	223
6900	374	7370	357	7840	234
6910	362	7380	352	7850	245
6920	387	7390	365	7860	215
6930	422	7400	330	7870	222
6940	394	7410	324	7880	250
6950	355	7420	326	7890	212
6960	367	7430	303	7900	211
6970	327	7440	315	7910	244
6980	342	7450	274	7920	277
6990	326	7460	269	7930	225
7000	322	7470	252	7940	255
7010	342	7480	265	7950	247
7020	336	7490	251	7960	260
7030	322	7500	243	7970	235
7040	338	7510	264	7980	243
7050	321	7520	257	7990	201
7060	328	7530	265	8000	235
7070	298	7540	285	8010	219
7080	329	7550	277	8020	235
7090	364	7560	271	8030	216
7100	341	7570	281	8040	213
7110	303	7580	295	8050	232
7120	305	7590	257	8060	229
7130	342	7600	325	8070	236
7140	342	7610	354	8080	219
7150	354	7620	331	8090	245
7160	479	7630	354	8100	230

8110	242
8120	222
8130	211
8140	209
8150	267
8160	214
8170	224
8180	224
8190	210
8200	259
8210	238
8220	220
8230	273
8240	298
8250	261
8260	322
8270	335
8280	364
8290	397
8300	420
8310	357
8320	361
8330	265
8340	269
8350	251
8360	259

Raw Diffraction Data for $SmD_{2.89}$ at λ =1.275

1090	92	1560	103	2030	94
1100	107	1570	109	2040	102
1110	100	1580	97	2050	116
1120	96	1590	104	2060	101
1130	80	1600	105	2070	99
1140	88	1610	115	2080	107
1150	84	1620	89	2090	95
1160	90	1630	110	2100	113
1170	92	1640	98	2110	78
1180	83	1650	99	2120	91
1190	79	1660	97	2130	116
1200	90	1670	106	2140	132
1210	71	1680	94	2150	130
1220	90	1690	108	2160	154
1230	77	1700	99	2170	160
1240	77	1710	108	2180	131
1250	83	1720	126	2190	125
1260	74	1730	119	2200	116
1270	87	1740	110	2210	107
1280	84	1750	121	2220	107
1290	88	1760	108	2230	101
1300	73	1770	110	2240	119
1310	76	1780	113	2250	125
1320	80	1790	104	2260	131
1330	92	1800	99	2270	97
1340	94	1810	96	2280	97
1350	76	1820	102	2290	92
1360	79	1830	114	2300	88
1370	92	1840	94	2310	89
1380	79	1850	105	2320	97
1390	87	1860	124	2330	109
1400	87	1870	113	2340	91
1410	90	1880	106	2350	99
1420	92	1890	130	2360	140
1430	87	1900	130	2370	155
1440	85	1910	112	2380	141
1450	106	1920	111	2390	148
1460	75	1930	118	2400	135
1470	93	1940	105	2410	114
1480	94	1950	131	2420	115
1490	97	1960	119	2430	85
1500	99	1970	111	2440	92
1510	101	1980	104	2450	87
1520	114	1990	122	2460	83
1530	95	2000	106	2470	99
1540	114	2010	102	2480	112
1550	114	2020	106	2490	83

2500	95	2960	89	3430	101
2510	90	2970	75	3440	100
2520	93	2980	83	3450	102
2530	87	2990	74	3460	91
2540	80	3000	79	3470	86
2550	70	3010	72	3480	93
2560	84	3020	94	3490	79
2570	84	3030	101	3500	97
2580	91	3040	101	3510	101
2590	84	3050	80	3520	83
2600	83	3060	78	3530	94
2610	87	3070	91	3540	86
2620	94	3080	97	3550	107
2630	110	3090	83	3560	82
2640	84	3100	101	3570	94
2650	88	3110	105	3580	95
2660	90	3120	91	3590	96
2670	80	3130	103	3600	100
2680	76	3140	114	3610	87
2690	66	3150	130	3620	93
2700	94	3160	103	3630	91
2710	89	3170	150	3640	93
2720	78	3180	112	3650	99
2730	79	3190	127	3660	97
2740	84	3200	110	3670	84
2750	66	3210	100	3680	85
2760	86	3220	103	3690	114
2770	91	3230	104	3700	88
2780	82	3240	101	3710	95
2790	77	3250	109	3720	81
2800	102	3260	108	3730	91
2810	84	3270	95	3740	92
2820	73	3280	101	3750	99
2830	78	3290	120	3760	87
2840	81	3300	100	3770	84
2850	79	3310	113	3780	84
2860	80	3320	106	3790	95
2870	75	3330	130	3800	96
2880	77	3340	119	3810	73
2890	81	3350	121	3820	109
2900	73	3360	127	3830	90
2910	86	3370	126	3840	92
2920	78	3380	147	3850	113
2930	64	3390	131	3860	133
2940	77	3400	98	3870	196
2950	79	3410	110	3880	234
		3420	86	3890	223

3900	277	4370	81	4840	96
3910	418	4380	95	4850	107
3920	593	4390	85	4860	89
3930	754	4400	87	4870	76
3940	940	4410	89	4880	94
3950	887	4420	95	4890	81
3960	805	4430	91	4900	85
3970	586	4440	109	4910	82
3980	449	4450	66	4920	77
3990	379	4460	107	4930	98
4000	325	4470	88	4940	99
4010	332	4480	104	4950	111
4020	357	4490	94	4960	80
4030	308	4500	103	4970	95
4040	230	4510	98	4980	95
4050	163	4520	123	4990	82
4060	137	4530	120	5000	97
4070	98	4540	144	5010	102
4080	104	4550	153	5020	89
4090	98	4560	141	5030	74
4100	118	4570	146	5040	88
4110	102	4580	134	5050	79
4120	111	4590	108	5060	83
4130	112	4600	129	5070	104
4140	100	4610	120	5080	95
4150	95	4620	119	5090	76
4160	90	4630	128	5100	87
4170	106	4640	140	5110	82
4180	93	4650	144	5120	96
4190	85	4660	161	5130	114
4200	95	4670	136	5140	81
4210	110	4680	149	5150	88
4220	83	4690	133	5160	111
4230	84	4700	114	5170	93
4240	94	4710	115	5180	95
4250	95	4720	113	5190	108
4260	92	4730	106	5200	86
4270	119	4740	111	5210	91
4280	87	4750	110	5220	92
4290	84	4760	95	5230	117
4300	85	4770	86	5240	102
4310	89	4780	68	5250	85
4320	79	4790	97	5260	100
4330	74	4800	82	5270	88
4340	89	4810	93	5280	109
4350	73	4820	75	5290	108
4360	74	4830	93	5300	109

5310	93	5780	303	6250	234
5320	94	5790	223	6260	219
5330	101	5800	195	6270	312
5340	110	5810	188	6280	305
5350	104	5820	168	6290	308
5360	105	5830	160	6300	276
5370	83	5840	122	6310	308
5380	108	5850	139	6320	284
5390	88	5860	188	6330	330
5400	92	5870	178	6340	269
5410	101	5880	115	6350	311
5420	93	5890	183	6360	288
5430	102	5900	184	6370	294
5440	98	5910	145	6380	287
5450	102	5920	158	6390	226
5460	108	5930	174	6400	258
5470	115	5940	155	6410	237
5480	108	5950	141	6420	253
5490	136	5960	164	6430	290
5500	106	5970	181	6440	259
5510	111	5980	145	6450	199
5520	104	5990	147	6460	140
5530	117	6000	144	6470	149
5540	103	6010	169	6480	153
5550	138	6020	124	6490	158
5560	120	6030	170	6500	146
5570	103	6040	154	6510	150
5580	129	6050	186	6520	137
5590	99	6060	200	6530	179
5600	148	6070	152	6540	172
5610	134	6080	154	6550	156
5620	132	6090	204	6560	155
5630	155	6100	210	6570	156
5640	123	6110	204	6580	129
5650	161	6120	189	6590	158
5660	188	6130	231	6600	147
5670	179	6140	217	6610	135
5680	193	6150	234	6620	154
5690	241	6160	215	6630	165
5700	224	6170	255	6640	153
5710	264	6180	208	6650	166
5720	264	6190	245	6660	136
5730	281	6200	232	6670	144
5740	301	6210	196	6680	159
5750	309	6220	206	6690	158
5760	308	6230	244	6700	157
5770	250	6240	222	6710	145

6720	155	7200	439	7670	143
6730	155	7210	363	7680	142
6740	156	7220	333	7690	164
6750	172	7230	266	7700	148
6760	129	7240	230	7710	117
6770	143	7250	223	7720	142
6780	145	7260	203	7730	110
6790	176	7270	176	7740	128
6800	142	7280	149	7750	112
6810	145	7290	139	7760	120
6820	121	7300	152	7770	132
6830	131	7310	160	7780	114
6840	139	7320	169	7790	102
6850	138	7330	165	7800	106
6860	154	7340	156	7810	132
6870	154	7350	175	7820	128
6880	154	7360	162	7830	126
6890	152	7370	167	7840	106
6900	149	7380	133	7850	119
6910	136	7390	162	7860	129
6920	147	7400	154	7870	116
6930	122	7410	155	7880	97
6940	149	7420	131	7890	118
6950	140	7430	117	7900	105
6960	127	7440	114	7910	119
6970	122	7450	118	7920	99
6980	135	7460	131	7930	139
6990	151	7470	124	7940	108
7000	148	7480	113	7950	121
7010	136	7490	120	7960	122
7020	143	7500	118	7970	105
7030	158	7510	135	7980	119
7040	169	7520	145	7990	124
7050	171	7530	145	8000	104
7060	182	7540	155	8010	106
7070	144	7550	155	8020	134
7080	155	7560	205	8030	136
7090	172	7570	143	8040	83
7110	207	7580	199	8050	107
7120	221	7590	203	8060	119
7130	269	7600	201	8070	120
7140	336	7610	207	8080	131
7150	384	7620	184	8090	115
7160	182	7630	168	8100	120
7170	499	7640	149	8110	109
7180	506	7650	153	8120	120
7190	434	7660	180	8130	120

8140	110	8610	126
8150	121	8620	131
8160	136	8630	111
8170	131	8640	120
8180	142	8650	134
8190	115	8660	148
8200	149	8670	140
8210	164	8680	148
8220	156	8690	132
8230	156	8700	132
8240	150	8710	90
8250	168	8720	123
8260	170	8730	115
8270	163	8740	127
8280	151	8750	124
8290	149	8760	122
8300	155	8770	132
8310	123	8780	115
8320	128	8790	133
8330	133	8800	134
8340	122	8810	105
8350	125	8820	147
8360	127	8830	127
8370	146	8840	141
8380	118	8850	164
8390	123	8860	119
8400	146	8870	137
8410	135	8880	155
8420	136	8890	133
8430	144	8900	129
8440	149	8910	173
8450	156	8920	169
8460	158	8930	169
8470	155	8940	140
8480	204	8950	164
8490	175	8960	143
8500	217	8970	139
8510	218	8980	161
8520	239	8990	166
8530	232	9000	157
8540	236		
8550	206		
8560	156		
8570	130		
8580	143		
8590	144		
8600	117		

Raw Diffraction Data for $SmD_{2.99}$ at λ =1.275

1000	41	1450	42	1920	47
1010	57	1470	43	1930	34
1020	37	1480	54	1940	41
1030	37	1490	26	1950	40
1040	54	1500	50	1960	48
1050	38	1510	52	1970	37
1060	43	1520	48	1980	53
1070	35	1530	53	1990	43
1080	45	1540	46	2000	44
1090	42	1550	43	2010	48
1100	45	1560	45	2020	39
1110	47	1570	45	2030	41
1120	55	1580	48	2040	36
1130	54	1590	52	2050	42
1140	39	1600	45	2060	53
1150	46	1610	41	2070	52
1160	39	1620	39	2080	57
1170	39	1630	45	2090	44
1180	39	1640	57	2100	42
1190	38	1650	51	2110	41
1200	38	1660	39	2120	49
1210	47	1670	52	2130	39
1220	41	1680	48	2140	34
1230	55	1690	43	2150	40
1240	47	1700	46	2160	33
1250	48	1710	39	2170	43
1260	40	1720	51	2180	45
1270	56	1730	43	2190	44
1280	36	1740	41	2200	36
1290	41	1750	44	2210	43
1300	46	1760	45	2220	41
1310	42	1770	43	2230	35
1320	41	1780	48	2240	40
1330	50	1790	40	2250	49
1340	29	1800	36	2260	44
1350	41	1810	62	2270	34
1360	44	1820	45	2280	50
1370	44	1830	54	2290	53
1380	44	1840	55	2300	44
1390	35	1850	51	2310	50
1400	43	1860	49	2320	47
1410	34	1870	37	2330	37
1420	47	1880	58	2340	47
1430	45	1890	32	2350	39
1440	45	1900	39	2360	41
1450	53	1910	42	2370	41

2380	49	2840	35	3300	49
2390	46	2850	31	3310	38
2400	40	2860	31	3320	36
2410	49	2870	31	3330	48
2420	44	2880	30	3340	43
2430	37	2890	30	3350	40
2440	40	2900	38	3360	51
2450	46	2910	42	3370	51
2460	35	2920	37	3380	59
2470	55	2930	25	3390	57
2480	40	2940	44	3400	62
2490	53	2950	33	3410	73
2500	46	2960	29	3420	60
2510	47	2970	34	3430	79
2520	39	2980	27	3440	71
2530	40	2990	33	3450	51
2540	45	3000	31	3460	55
2550	35	3010	24	3470	60
2560	50	3020	29	3480	65
2570	36	3030	28	3490	51
2580	37	3040	35	3500	56
2590	32	3050	37	3510	56
2600	51	3060	31	3520	47
2610	41	3070	30	3530	55
2620	46	3080	26	3540	41
2630	51	3090	21	3550	44
2640	42	3100	29	3560	48
2650	55	3110	37	3570	43
2660	46	3120	33	3580	54
2670	43	3130	30	3590	44
2680	33	3140	40	3600	41
2690	38	3150	48	3610	55
2700	34	3160	45	3620	49
2710	41	3170	46	3630	48
2720	35	3180	43	3640	44
2730	34	3190	42	3650	38
2740	31	3200	44	3660	50
2750	29	3210	46	3670	41
2760	41	3220	39	3680	56
2770	32	3230	41	3690	58
2780	37	3240	51	3700	45
2790	34	3250	43	3710	61
2800	33	3260	35	3720	43
2810	37	3270	42	3730	45
2820	41	3280	43	3740	57
2830	35	3290	47	3750	47

3760	34	4220	52	4680	65
3770	48	4230	44	4690	55
3780	54	4240	45	4700	54
3790	31	4250	42	4710	50
3800	50	4260	52	4720	42
3810	53	4270	46	4730	55
3820	44	4280	38	4740	70
3830	54	4290	40	4750	56
3840	52	4300	38	4760	53
3850	55	4310	55	4770	60
3860	39	4320	43	4780	61
3870	55	4330	50	4790	60
3880	64	4340	37	4800	55
3890	49	4350	44	4810	57
3900	70	4360	48	4820	46
3910	63	4370	44	4830	57
3920	87	4380	55	4840	54
3930	154	4390	46	4850	47
3940	218	4400	38	4860	43
3950	292	4410	51	4870	43
3960	342	4420	40	4880	42
3970	355	4430	47	4890	67
3980	303	4440	63	4900	57
3990	240	4450	32	4910	49
4000	242	4460	56	4920	40
4010	254	4470	44	4930	52
4020	297	4480	51	4940	49
4030	287	4490	48	4950	51
4040	303	4500	41	4960	45
4050	242	4510	41	4970	62
4060	168	4520	32	4980	53
4070	130	4530	38	4990	60
4080	111	4540	51	5000	57
4090	80	4550	77	5010	56
4100	60	4560	82	5020	53
4110	63	4570	104	5030	52
4120	63	4580	102	5040	48
4130	55	4590	105	5050	50
4140	59	4600	116	5060	55
4150	54	4610	70	5070	59
4160	53	4620	77	5080	66
4170	53	4630	55	5090	57
4180	50	4640	54	5100	50
4190	58	4650	79	5110	52
4200	44	4660	68	5120	51
4210	35	4670	65	5130	54

5140	52	5600	59	6060	68
5150	45	5610	63	6070	72
5160	46	5620	66	6080	84
5170	54	5630	74	6090	87
5180	46	5640	54	6100	83
5190	39	5650	77	6110	88
5200	52	5660	65	6120	84
5210	53	5670	62	6130	103
5220	53	5680	74	6140	91
5230	57	5690	87	6150	104
5240	57	5700	71	6160	97
5250	69	5710	81	6170	108
5260	50	5720	72	6180	113
5270	54	5730	79	6190	97
5280	80	5740	74	6200	93
5290	60	5750	125	6210	90
5300	60	5760	116	6220	108
5310	51	5770	165	6230	96
5320	72	5780	187	6240	105
5330	63	5790	173	6250	94
5340	54	5800	206	6260	105
5350	65	5810	182	6270	94
5360	67	5820	152	6280	101
5370	54	5830	122	6290	116
5380	58	5840	124	6300	116
5390	51	5850	96	6310	110
5400	64	5860	83	6320	88
5410	71	5870	75	6330	103
5420	56	5880	77	6340	90
5430	62	5890	86	6350	103
5440	58	5900	83	6360	116
5450	47	5910	65	6370	130
5460	61	5920	77	6380	138
5470	56	5930	78	6390	124
5480	60	5940	69	6400	121
5490	67	5950	83	6410	128
5500	64	5960	68	6420	110
5510	60	5970	90	6430	104
5520	63	5980	79	6440	127
5530	61	5990	87	6450	108
5540	66	6000	70	6460	100
5550	57	6010	80	6470	106
5560	62	6020	79	6480	100
5570	58	6030	67	6490	82
5580	62	6040	82	6500	106
5590	65	6050	87	6510	108

6520	108	6980	94	7440	97
6530	112	6990	98	7450	97
6540	124	7000	102	7460	84
6550	118	7010	88	7470	86
6560	107	7020	80	7480	86
6570	97	7030	79	7490	68
6580	135	7040	93	7500	95
6590	108	7050	86	7510	68
6600	121	7060	95	7520	89
6610	92	7070	94	7530	76
6620	130	7080	96	7540	82
6630	115	7090	106	7550	105
6640	107	7100	111	7560	110
6650	92	7110	93	7570	113
6660	104	7120	105	7580	125
6670	104	7130	113	7590	130
6680	118	7140	98	7600	138
6690	102	7150	96	7610	138
6700	124	7160	95	7620	148
6710	97	7170	134	7630	134
6720	110	7180	152	7640	135
6730	101	7190	186	7650	136
6740	129	7200	195	7660	130
6750	124	7210	233	7670	104
6760	125	7220	232	7680	103
6770	108	7230	279	7690	106
6780	123	7240	301	7700	82
6790	104	7250	279	7710	79
6800	105	7260	246	7720	74
6810	109	7270	227	7730	76
6820	118	7280	221	7740	66
6830	96	7290	158	7750	95
6840	101	7300	142	7760	90
6850	104	7310	120	7770	70
6860	105	7320	127	7780	99
6870	104	7330	85	7790	68
6880	112	7340	117	7800	80
6890	102	7350	131	7810	74
6900	102	7360	118	7820	71
6910	85	7370	115	7830	69
6920	107	7380	126	7840	72
6930	117	7390	121	7850	63
6940	125	7400	115	7860	69
6950	117	7410	111	7870	79
6960	90	7420	105	7880	68
6970	107	7430	120	7890	64

7900	75	8350	89	8820	88
7910	84	8370	85	8830	73
7920	78	8380	83	8840	82
7930	79	8390	73	8850	56
7940	67	8400	72	8860	92
7950	55	8410	96	8870	77
7960	70	8420	81	8880	88
7970	80	8430	81	8890	85
7980	63	8440	77	8900	97
7990	74	8450	95	8910	105
8000	74	8460	81	8920	91
8010	85	8470	78	8930	117
8020	84	8480	85	8940	98
8030	83	8490	95	8950	119
8040	59	8500	104	8960	115
8050	78	8510	84	8970	111
8060	66	8520	124	8980	105
8070	79	8530	102	8990	103
8080	80	8540	122	9000	112
8090	82	8550	128		
8100	68	8560	134		
8110	71	8570	127		
8120	62	8580	137		
8130	84	8590	129		
8140	78	8600	122		
8150	69	8610	111		
8160	74	8620	95		
8170	67	8630	100		
8180	93	8640	80		
8190	74	8650	88		
8200	81	8660	90		
8210	93	8670	85		
8220	70	8680	71		
8230	95	8690	90		
8240	95	8700	102		
8250	98	8710	89		
8260	132	8720	104		
8270	129	8730	90		
8280	161	8740	92		
8290	145	8750	104		
8300	150	8760	99		
8310	139	8770	104		
8320	130	8780	79		
8330	101	8790	77		
8340	107	8800	94		
8350	91	8810	74		

APPENDIX G

Space Groups 194 and 225
$P6_3/mmC$ and $Fm3m$

Origin at centre ($m3m$)

Number of positions, Wyckoff notation, point symmetry			Co-ordinates of equivalent positions $(0,0,0;\ 0,\frac{1}{2},\frac{1}{2};\ \frac{1}{2},0,\frac{1}{2};\ \frac{1}{2},\frac{1}{2},0)+$	Conditions limiting possible reflections
				General:
192	l	1	$x,y,z;\ z,x,y;\ y,z,x;\ x,z,y;\ y,x,z;\ z,y,x;$ $x,\bar{y},\bar{z};\ z,\bar{x},\bar{y};\ y,\bar{z},\bar{x};\ x,\bar{z},\bar{y};\ y,\bar{x},\bar{z};\ z,\bar{y},\bar{x};$ $\bar{x},\bar{y},\bar{z};\ \bar{z},x,\bar{y};\ \bar{y},z,\bar{x};\ \bar{x},z,\bar{y};\ \bar{y},x,\bar{z};\ \bar{z},y,\bar{x};$ $\bar{x},\bar{y},z;\ \bar{z},\bar{x},y;\ \bar{y},\bar{z},x;\ \bar{x},\bar{z},y;\ \bar{y},\bar{x},z;\ \bar{z},\bar{y},x;$ $\bar{x},\bar{y},\bar{z};\ \bar{z},\bar{x},\bar{y};\ \bar{y},\bar{z},\bar{x};\ \bar{x},\bar{z},\bar{y};\ \bar{y},\bar{x},\bar{z};\ \bar{z},\bar{y},\bar{x};$ $\bar{x},y,z;\ \bar{z},x,y;\ \bar{y},z,x;\ \bar{x},z,y;\ \bar{y},x,z;\ \bar{z},y,x;$ $x,\bar{y},z;\ z,\bar{x},y;\ y,\bar{z},x;\ x,\bar{z},y;\ y,\bar{x},z;\ z,\bar{y},x;$ $x,y,\bar{z};\ z,x,\bar{y};\ y,z,\bar{x};\ x,z,\bar{y};\ y,x,\bar{z};\ z,y,\bar{x}.$	hkl: $h+k,k+l,(l+h)=2n$; C hhl: $(l+h=2n)$; C $0kl$: $(k,l=2n)$; C
				Special: as above, plus
96	k	m	$x,x,z;\ z,x,x;\ x,z,x;\ \bar{x},\bar{x},\bar{z};\ \bar{z},\bar{x},\bar{x};\ \bar{x},\bar{z},\bar{x};$ $x,\bar{x},\bar{z};\ z,\bar{x},\bar{x};\ x,\bar{z},\bar{x};\ \bar{x},x,z;\ \bar{z},x,x;\ \bar{x},z,x;$ $\bar{x},x,\bar{z};\ \bar{z},x,\bar{x};\ \bar{x},z,\bar{x};\ x,\bar{x},z;\ z,\bar{x},x;\ x,\bar{z},x;$ $\bar{x},\bar{x},z;\ \bar{z},\bar{x},x;\ \bar{x},\bar{z},x;\ x,x,\bar{z};\ z,x,\bar{x};\ x,z,\bar{x}.$	no extra conditions
96	j	m	$0,y,z;\ z,0,y;\ y,z,0;\ 0,z,y;\ y,0,z;\ z,y,0;$ $0,\bar{y},\bar{z};\ \bar{z},0,\bar{y};\ \bar{y},\bar{z},0;\ 0,\bar{z},\bar{y};\ \bar{y},0,\bar{z};\ \bar{z},\bar{y},0;$ $0,y,\bar{z};\ \bar{z},0,y;\ y,\bar{z},0;\ 0,\bar{z},y;\ y,0,\bar{z};\ \bar{z},y,0;$ $0,\bar{y},z;\ z,0,\bar{y};\ \bar{y},z,0;\ 0,z,\bar{y};\ \bar{y},0,z;\ z,\bar{y},0.$	
	i	mm	$\frac{1}{2},x,x;\ x,\frac{1}{2},x;\ x,x,\frac{1}{2};\ \frac{1}{2},x,\bar{x};\ \bar{x},\frac{1}{2},x;\ x,\bar{x},\frac{1}{2};$ $\frac{1}{2},\bar{x},\bar{x};\ \bar{x},\frac{1}{2},\bar{x};\ \bar{x},\bar{x},\frac{1}{2};\ \frac{1}{2},\bar{x},x;\ x,\frac{1}{2},\bar{x};\ \bar{x},x,\frac{1}{2}.$	
	h	mm	$0,x,x;\ x,0,x;\ x,x,0;\ 0,x,\bar{x};\ \bar{x},0,x;\ x,\bar{x},0;$ $0,\bar{x},\bar{x};\ \bar{x},0,\bar{x};\ \bar{x},\bar{x},0;\ 0,\bar{x},x;\ x,0,\bar{x};\ \bar{x},x,0.$	
48	g	mm	$x,\frac{1}{4},\frac{1}{4};\ \frac{1}{4},x,\frac{1}{4};\ \frac{1}{4},\frac{1}{4},x;\ x,\frac{1}{4},\frac{3}{4};\ \frac{3}{4},x,\frac{1}{4};\ \frac{1}{4},\frac{3}{4},x;$ $\bar{x},\frac{1}{4},\frac{1}{4};\ \frac{1}{4},\bar{x},\frac{1}{4};\ \frac{1}{4},\frac{1}{4},\bar{x};\ \bar{x},\frac{1}{4},\frac{3}{4};\ \frac{3}{4},\bar{x},\frac{1}{4};\ \frac{1}{4},\frac{3}{4},\bar{x}.$	hkl: $h,(k,l)=2n$
32	f	$3m$	$x,x,x;\ x,\bar{x},\bar{x};\ \bar{x},x,\bar{x};\ \bar{x},\bar{x},x;$ $\bar{x},\bar{x},\bar{x};\ \bar{x},x,x;\ x,\bar{x},x;\ x,x,\bar{x}.$	no extra conditions
24	e	$4mm$	$x,0,0;\ 0,x,0;\ 0,0,x;\ \bar{x},0,0;\ 0,\bar{x},0;\ 0,0,\bar{x}.$	
24	d	mmm	$0,\frac{1}{4},\frac{1}{4};\ \frac{1}{4},0,\frac{1}{4};\ \frac{1}{4},\frac{1}{4},0;\ 0,\frac{1}{4},\frac{3}{4};\ \frac{3}{4},0,\frac{1}{4};\ \frac{1}{4},\frac{3}{4},0.$	hkl: $h,(k,l)=2n$
8	c	$\bar{4}3m$	$\frac{1}{4},\frac{1}{4},\frac{1}{4};\ \frac{3}{4},\frac{3}{4},\frac{3}{4}.$	
4	b	$m3m$	$\frac{1}{2},\frac{1}{2},\frac{1}{2}.$	no extra conditions
1	a	$m3m$	$0,0,0.$	

$P6_3/mmc$ D_{6h}^4 No. 194 $P6_3/m\,2/m\,2/c$ $6/m\,m\,m$ Hexagonal

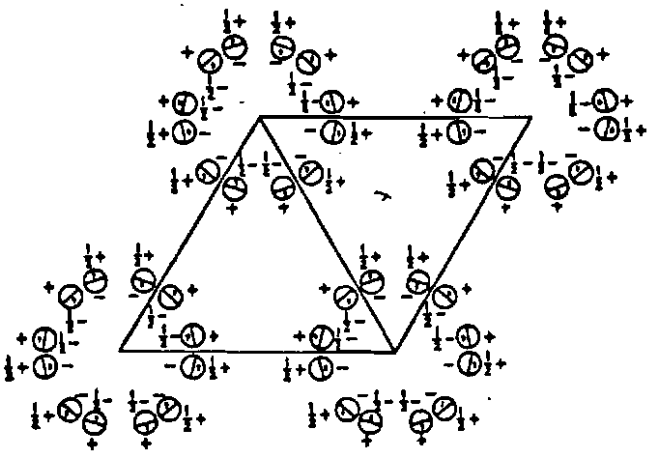

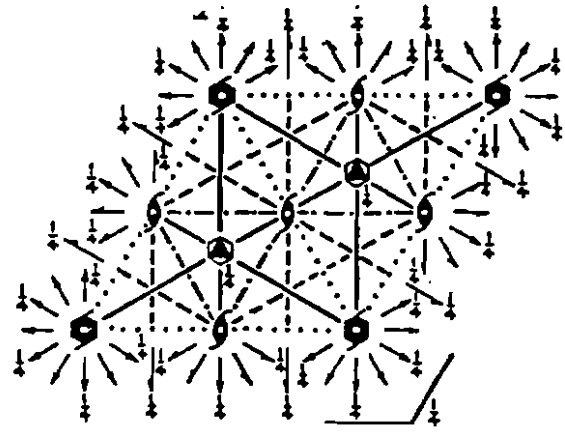

Origin at centre ($\bar{3}m1$)

Number of positions, Wyckoff notation, and point symmetry			Co-ordinates of equivalent positions	Conditions limiting possible reflections
				General:
24	l	1	x,y,z; $\bar{y},x-y,z$; $y-x,\bar{x},z$; $\bar{y},\bar{x},z$; $x,x-y,z$; $y-x,y,z$; $\bar{x},\bar{y},\bar{z}$; $y,y-x,\bar{z}$; $x-y,x,\bar{z}$; $y,x,\bar{z}$; $\bar{x},y-x,\bar{z}$; $x-y,\bar{y},\bar{z}$; $\bar{x},\bar{y},\frac{1}{2}+z$; $y,y-x,\frac{1}{2}+z$; $x-y,x,\frac{1}{2}+z$; $x,y,\frac{1}{2}-z$; $\bar{y},x-y,\frac{1}{2}-z$; $y-x,\bar{x},\frac{1}{2}-z$; $y,x,\frac{1}{2}+z$; $\bar{x},y-x,\frac{1}{2}+z$; $x-y,\bar{y},\frac{1}{2}+z$; $\bar{y},\bar{x},\frac{1}{2}-z$; $x,x-y,\frac{1}{2}-z$; $y-x,y,\frac{1}{2}-z$.	$hkil$: No conditions $hh2hl$: $l=2n$ $h\bar{h}0l$: No conditions
				Special: as above, plus
12	k	m	$x,2x,z$; $2\bar{x},\bar{x},z$; $x,\bar{x},z$; $\bar{x},2\bar{x},\bar{z}$; $2x,x,\bar{z}$; $\bar{x},x,\bar{z}$; $\bar{x},2\bar{x},\frac{1}{2}+z$; $2x,x,\frac{1}{2}+z$; $\bar{x},x,\frac{1}{2}+z$; $x,2x,\frac{1}{2}-z$; $2\bar{x},\bar{x},\frac{1}{2}-z$; $x,\bar{x},\frac{1}{2}-z$.	no extra conditions
12	j	m	$x,y,\frac{1}{4}$; $\bar{y},x-y,\frac{1}{4}$; $y-x,\bar{x},\frac{1}{4}$; $\bar{y},\bar{x},\frac{1}{4}$; $x,x-y,\frac{1}{4}$; $y-x,y,\frac{1}{4}$; $\bar{x},\bar{y},\frac{3}{4}$; $y,y-x,\frac{3}{4}$; $x-y,x,\frac{3}{4}$; $y,x,\frac{3}{4}$; $\bar{x},y-x,\frac{3}{4}$; $x-y,\bar{y},\frac{3}{4}$.	
12	i	2	$x,0,0$; $0,x,0$; $\bar{x},\bar{x},0$; $x,0,\frac{1}{2}$; $0,x,\frac{1}{2}$; $\bar{x},\bar{x},\frac{1}{2}$; $\bar{x},0,0$; $0,\bar{x},0$; $x,x,0$; $\bar{x},0,\frac{1}{2}$; $0,\bar{x},\frac{1}{2}$; $x,x,\frac{1}{2}$.	$hkil$: $l=2n$
6	h	mm	$x,2x,\frac{1}{4}$; $2\bar{x},\bar{x},\frac{1}{4}$; $x,\bar{x},\frac{1}{4}$; $\bar{x},2\bar{x},\frac{3}{4}$; $2x,x,\frac{3}{4}$; $\bar{x},x,\frac{3}{4}$.	no extra conditions
6	g	$2/m$	$\frac{1}{2},0,0$; $0,\frac{1}{2},0$; $\frac{1}{2},\frac{1}{2},0$; $\frac{1}{2},0,\frac{1}{2}$; $0,\frac{1}{2},\frac{1}{2}$; $\frac{1}{2},\frac{1}{2},\frac{1}{2}$.	$hkil$: $l=2n$
4	f	$3m$	$\frac{1}{3},\frac{2}{3},z$; $\frac{2}{3},\frac{1}{3},\bar{z}$; $\frac{2}{3},\frac{1}{3},\frac{1}{2}+z$; $\frac{1}{3},\frac{2}{3},\frac{1}{2}-z$.	$hkil$: If $h-k=3n$, then $l=2n$
4	e	$3m$	$0,0,z$; $0,0,\bar{z}$; $0,0,\frac{1}{2}+z$; $0,0,\frac{1}{2}-z$.	$hkil$: $l=2n$

Hexagonal $6/m\ m\ m$ $P\,6_3/m\,2/m\,2/c$ No. 194 $P\,6_3/m\,m\,c$ D_{6h}^4

(continued)

2	d	$\bar{6}m2$	$\frac{1}{3},\frac{2}{3},\frac{3}{4}$;	$\frac{2}{3},\frac{1}{3},\frac{1}{4}$.	*hkil*: If $h-k=3n$, then $l=2n$
2	c	$\bar{6}m2$	$\frac{1}{3},\frac{2}{3},\frac{1}{4}$;	$\frac{2}{3},\frac{1}{3},\frac{3}{4}$.	
2	b	$\bar{6}m2$	$0,0,\frac{1}{4}$;	$0,0,\frac{3}{4}$.	*hkil*: $l=2n$
2	a	$\bar{3}m$	$0,0,0$;	$0,0,\frac{1}{2}$.	